atmosphere

MDPI

Article

Comparison of the Impact of Ship Emissions in Northern Europe and Eastern China

Daniel A. Schwarzkopf [1,*], Ronny Petrik [1], Volker Matthias [1,*], Markus Quante [1,*], Guangyuan Yu [2] and Yan Zhang [2]

[1] Helmholtz-Zentrum Hereon, Institute of Coastal Environmental Chemistry, Max-Planck-Straße 1, 21502 Geesthacht, Germany; ronny.petrik@hereon.de (R.P.); volker.matthias@hereon.de (V.M.); markus.quante@hereon.de (M.Q.)

[2] Institute of Atmospheric Sciences, Fudan University, Shanghai 200438, China; 19110740001@fudan.edu.cn (G.Y.); yan_zhang@fudan.edu.cn (Y.Z.)

* Correspondence: daniel.schwarzkopf@hereon.de

Abstract: It is well known that ship emissions contribute significantly to atmospheric pollution. However, the impact on air quality can regionally vary, as influenced by parameters such as the composition of the regional shipping fleet, state of background atmospheric pollution, and meteorological aspects. This study compared two regions with high shipping densities in 2015. These include the North and Baltic Seas in Europe and the Yellow and East China Seas in China. Here, a key focal point is an evaluation of differences and similarities of the impacts of ship emissions under different environmental conditions, particularly between regions with medium (Europe) and high air pollution (China). To assess this, two similarly performed chemical transport model runs were carried out with highly resolved bottom-up ship emission inventories for northern Europe and China, calculated with the recently developed MoSES model, publicly available emissions data for nonshipping sources (EDGAR, MEIC). The performance of the model was evaluated against measurement data recorded at coastal stations. Annual averages at affected coastal regions for NO_2, SO_2, O_3 and $PM_{2.5}$ were modeled in Europe to be 3, below 0.3, 2.5, 1 and in China 3, 2, 2–8, 1.5, respectively, all given in $\mu g/m^3$. In highly affected regions, such as large harbors, the contributions of ship-related emissions modeled in Europe were 15%, 0.3%, −12.5%, 1.25% and in China were 15%, 6%, −7.5%, 2%, respectively. Absolute pollutant concentrations from ships were modeled slightly higher in China than in Europe, albeit the relative impact was smaller in China due to higher emissions from other sectors. The different climate zones of China and the higher level of atmospheric pollution were found to seasonally alter the chemical transformation processes of ship emissions. Especially in northern China, high PM concentrations during winter were found to regionally inhibit the transformation of ship exhausts to secondary PM, and reduce the impact of ship-related aerosols, compared to Europe.

Keywords: ship; emissions; emission inventory; Europe; China; comparison; air quality; modeling; CMAQ; MoSES

Citation: Schwarzkopf, D.A.; Petrik, R.; Matthias, V.; Quante, M.; Yu, G., Zhang, Y. Comparison of the Impact of Ship Emissions in Northern Europe and Eastern China. *Atmosphere* **2022**, *13*, 894. https://doi.org/10.3390/atmos13060894

Academic Editor: Sofia Sousa

Received: 7 May 2022
Accepted: 27 May 2022
Published: 31 May 2022

1. Introduction

For economic reasons, the maritime sector has long been the first choice for freight transport across the globe. Although ships are a relatively environmentally friendly mode of transport, when considering cargo volume per fuel consumption, the steadily growing global merchandise turnover and the associated shipping activity have led to a deterioration of air quality in many regions worldwide [1,2]. The combustion of fuel oil in ships is responsible for large amounts of air pollutants such as sulfur oxides (SO_X), nitrogen oxides (NO_X) and fine particulate matter ($PM_{2.5}$) [3]. Since ship emissions can be transported several hundred kilometers in the atmosphere, they can impact coastal regions and cities as well as regions further inland. In particular, $PM_{2.5}$ is well known to be responsible for

respiratory and cardiopulmonary diseases that can lead to premature death [4–7]. NO_X and SO_2 can transform to secondary PM and acidify the environment. In addition, NO_X is responsible for eutrophication and influences the formation of tropospheric ozone [8–10]. For these reasons, the regulation of ship emissions has been placed on the agenda by the International Maritime Organization (IMO) and many national authorities. The formulated legal framework is the International Convention for the Prevention of Pollution from Ships (MARPOL) Annex VI, in which global and regional regulations are adopted with the aim of preventing the negative effects from ship emissions [11]. In practice, the globally allowed fuel-sulfur content of marine fuels has been limited to 3.5% *m*/*m* (mass/mass) by MARPOL Annex VI. This cap was tightened to 0.5% at the beginning of 2020 [12,13].

Two regions that have been particularly affected by air degradation from ship emissions in recent decades are the North and Baltic Seas in northern Europe and the Bohai, Yellow and Eastern China Seas in East Asia. Both are regions with high shipping densities and large port cities that are tightly interconnected by global maritime freight transport.

Land-based sources of air pollution have been systematically reduced in Europe since the end of the last century, but air quality degradation from ship emissions has received necessary attention only in the last two decades [14–19]. Emissions from a growing shipping sector were met by the introduction of a sulfur emission control area (SECA) in the North and Baltic Seas, described in MARPOL Annex VI, in which the allowed fuel-sulfur content was limited to 1% *m*/*m* from 1. July 2010 and to 0.1% from the beginning of 2015 [12]. Many studies have been conducted that investigate the impact of ship emissions in the North and Baltic Seas on regional air quality and the regulating effect of control measures [5,15,19–24]. Furthermore, interdisciplinary projects have been initiated by the EU to investigate impacts in a comprehensive approach, e.g., Clean North Sea Shipping (CNSS) and Sustainable Shipping and the Environment of the Baltic Sea Region (SHEBA) [25,26].

In East Asia, the recent and rapid economic growth of the main regional actor China made it the world's largest emitter of air pollutants (18–35%) [27]. The Chinese government, well aware of the problem, set an annual average exposure limit for $PM_{2.5}$ of 35 $\mu g\ m^{-3}$ in 2012 [28]. From 2013 to 2017, the Chinese air degradation containment strategy was further tightened with the adopted "Plan on the Prevention and Control of Air Pollution" [29]. A monitoring system for air pollution was established, and industry, energy production and the transportation sector were adjusted to reduce ambient $PM_{2.5}$ concentrations by 28–40% in 2017 [30]. However, regulations for the shipping sector, one of the most prominent contributors to $PM_{2.5}$, remained incomplete [6]. China is home to seven of the ten largest container ports worldwide, and in 2019, almost 30% of the world's container port throughput (TEU) occurred there [31,32]. This freight volume is expected to increase in the near future due to China's 21st Century Maritime Silk Road Strategy and the recently ratified Free Trade Agreement Regional Comprehensive Economic Partnership (RCEP). A domestic emission control area (DECA), issued by the Chinese authorities, was enforced from the beginning of 2017 for berthing ships in 11 regional ports and from 2019 within 12 NM of the Chinese shoreline [33]. Within this DECA, the fuel-sulfur content is limited to a maximum of 0.5%. From the beginning of 2020, regulations were tightened to a maximum allowed fuel-sulfur of 0.1% for berthing ships. The effect of the DECA on air quality has been investigated in several studies. Liu et al. [34] determined that $PM_{2.5}$ and SO_2 concentrations in the Pearl River Delta (PRD) were reduced by 2.7% and 9.5%, respectively. Possible benefits from expanding the DECA have been modeled by Feng et al. [35]. Here, ships up to 96 NM from shore were found to contribute substantially to ship-originated $PM_{2.5}$. This finding is in accordance with the results from Zhao et al. [36], which showed that the DECA decreases the contribution of ship emissions to $PM_{2.5}$ by 71%, albeit a stricter fuel-sulfur limit and an expansion of the DECA to 100 NM from the coast may even achieve a reduction of 86%.

Although many studies exist concerning the impact of ships on air quality in China or Europe, no comparison between these two regions has been made to date. While the overarching problem is similar and many of the larger cargo ships can be encountered in either

region, regional differences result in a different impact. For example, domestic shipping activities such as fishing, freight/passenger transport and leisure shipping differ between Europe and China. The legislation targeting the control of ship emissions remains different in their details. In addition, higher pollutant emissions for nonshipping sources are found in China than in Europe. These can modulate the chemical and physical processes that emissions from shipping undergo in the atmosphere. Furthermore, different climate zones and regional weather phenomena, such as the East Asian monsoon and the rainy season in summer, affect the transport and deposition of ship exhausts. This study aims to assess the impact of ship emissions under consideration of these factors for otherwise analogously conducted air quality model runs in China and northern Europe. By comparing the results, conclusions are drawn concerning the behavior and physical/chemical transformation of pollutant species under different atmospheric conditions. These results should contribute to an understanding of the underlying processes and help in the formulation of future legislative control measures.

To assess this problem, the three-dimensional Community Multiscale Air Quality model (CMAQ) was set up (Section 2.1) and fed with emissions data from 2015 for both regions (Section 2.2). A highly temporally and spatially resolved ship emission inventory for China was created for this study, by a first comprehensive application of the Modular Ship Emission Modeling System (MoSES). A description of this model and an analogously created ship emission inventory for the European domain can be found in [37]. The description of the inventory for China and applied emission factors, as well as a comparison of the European and Chinese shipping fleets, can be found in Section 2.2.5. The performance of the model was evaluated by a comparison with air quality data measured at coastal stations (Section 3). Finally, the modeled concentration patterns of NO_2, SO_2, ozone and primary and secondary fine particulate matter in both domains are discussed (Section 4).

2. Materials and Methods

2.1. Model Simulations

2.1.1. Regions of Interest

Model domains were prepared for the two regions of interest for which this study compared the air quality impact of ship emissions. The region of northern Europe was covered by a domain hereafter referred to as SC12NSBS. It includes the North and Baltic Seas and is shown in Figure 1 (left). China was represented by a domain that is located in East Asia and is hereafter referred to as CNC12 (Figure 1 right). It includes the coastline of China, including the Bohai Sea, the Yellow Sea, the East China Sea and parts of the South China Sea. Both domains have the same extent in kilometers and include not only the main local shipping routes but also densely populated coastal regions, whose air quality is affected by ship exhausts. Two $12 \times 12\,km^2$ Lambert conformal grids were set up for the chemistry transport modeling (see Section 2.1.2 for details). Both grids consisted of 196×196 cells.

Two chemical transport simulations were performed for each domain: One represented a "base" case that included emissions from all sectors, and the other represented a "no ships" case, omitting ship emissions (see Section 2.2). The pollutant concentrations originating from shipping were then determined by the zero-out method, in which the "no ships" case is subtracted from the "base" case.

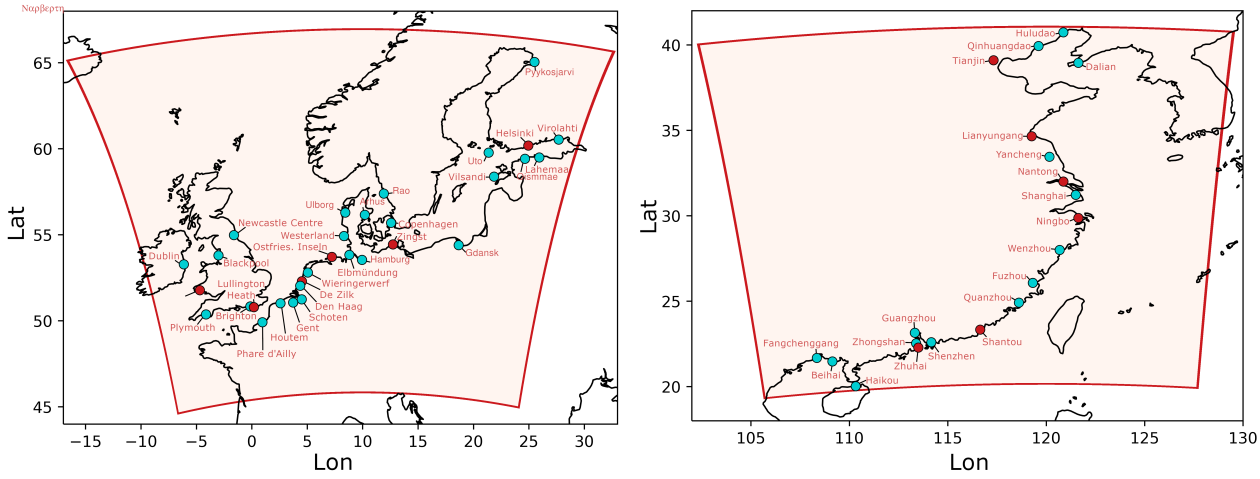

Figure 1. Modeled domains for northern Europe (**left**, SC12NSBS) and eastern China (**right**, CNC12) that were created for the comparison. Also shown are the air quality monitoring stations that were considered in an evaluation of the model performance. The red dots represent selected stations whose comparison data are exemplarily shown in Section 3. The data of the other stations can be found in the Appendix A and the Supplementary Materials.

2.1.2. Chemical Transport Model CMAQ-Setup and Forcing

The Community Multiscale Air Quality model (CMAQ) by Byun and Ching [38], Byun and Schere [39] in version 5.2, a chemistry transport model, was used and set up with the carbon bond 5 photochemical mechanism (CB05-TUCL) [40–42] and the AE6 aerosol mechanism. The CMAQ run was performed for 2015 after a previous spin-up time of 2 weeks to adapt to the initially homogeneous concentration fields and atmospheric conditions. The model considered 30 vertical layers from the ground surface up to a 100 hPa pressure level, which was located at approximately 8 km. Twenty of these layers were below an altitude of 2000 m. The lowest layer had a height of approximately 42 m and was located at approximately 21 m.

The simulations for China and Europe were nested into preceding, overarching CMAQ simulations that covered larger areas at a coarser resolution (36 km for Europe and 24 km for China) but used the same emission sources as the 12 km runs. The chemical conditions at the boundaries of these larger domains were taken from the Integrated Forecast System-Copernicus Atmosphere Monitoring Service (IFS-CAMS) analysis [43]. The data were available from the MARS archive at the European Centre for Medium-Range Weather Forecasts (ECMWF) and the CAMS Atmosphere Data Store [44]. Particle and gas concentration fields of the IFS-CAMS data are usually provided on a T511 spectral grid with 137 vertical levels, but due to retrieval issues, data on a 0.5° × 0.5° grid were used. The IFS-CAMS data were temporally and spatially remapped onto the boundary of the overarching domains. Chemical and particle species were converted to match the species used in CMAQ.

2.1.3. Meteorological Forcing

One important difference between the regions of interest was the characteristic of the atmospheric large-scale circulation. Therefore, reliable meteorological data are needed to calculate the transport and transformation of gas species and aerosol particles as realistically as possible. The meteorological forcing was realized by atmospheric simulations with the community model COSMO-CLM (version 5.0-clm15) [45], which is embedded into the COSMO model used for numerical weather prediction [46–48]. To simulate radiative transfer, an extension of the COSMO model for MACv2 transient aerosol climatology was used [49].

The atmospheric simulations were performed using forcing data from global models as initial and boundary conditions, i.e. the MERRA2 reanalysis [50] for the SC12NSBS domain and the JRA-55 reanalysis [51,52] for the CNC12 domain. The simulations for Europe were

performed on a grid with a resolution of 0.06° × 0.06°. To ensure that the atmospheric fields in the transient model integration were in accordance with the observations over the whole period, a nudging technique was used as described in Petrik et al. [53]. The reader is referred to this publication to find more information about the setup of the atmospheric model (setup "CCLM-oF-SN"). Regarding the simulations over eastern Asia, a domain with a resolution of 0.11° × 0.11° was used that consisted of 315 × 315 grid points.

The initialization of the soil proved a challenging task since the forcing data from the global model did not provide sufficient information consistent with the soil parameterization of the regional model. In the southeastern Asia region, the characteristics of soil drying and soil wetting are very different for the various climates. Different spin-up experiments for the soil were performed. The results suggested that at least one complete monsoon season and one complete winter season were needed: only then could the water reservoir be reasonably filled up, and the solution converged to a balanced state. In particular, the soil levels below one meter required a considerable amount of time. Additionally, the region of northern China, where precipitation events occur only rarely.

2.2. Emissions Data

The emissions data fed to CMAQ were compiled from different sources for 2015 and preprocessed to an hourly resolution.

2.2.1. Anthropogenic Land-Based Emissions for Europe

For the SC12NSBS domain in Europe, land-based emission data were based on the CAMS-REGAP-EU emission inventory for 2015 in version 3.1. The data set comprises annual anthropogenic emission totals for 13 GNFR sectors [54] (https://permalink.aeris-data.fr/CAMS-REG-AP, last accessed: 16 September 2021). The emissions were prepared utilizing the internally available Highly Modular Emission Model (HiMEMO). A temporal distribution up to a one-hour resolution was achieved using temporal profiles from the LOTOS-EUROS model, which were used to simulate a daily schedule of emissions from the GNFR sectors.

2.2.2. Anthropogenic Land-Based Emissions for China

For the CNC12 domain, emissions data from the Multiresolution Emission Inventory for China (MEIC) were used for nonshipping, land-based emission sources [55–62]. The monthly, gridded emissions of the MEIC inventory had an original spatial resolution of 0.25° × 0.25°. The emission inventory (EI) contained data for the five emission sectors: "Agriculture", "Industry", "Power", "Residential" and "Transportation". The following chemical species and compound groups were included: black carbon (BC), CO, NH_3, NO_X, organic compounds (OC), $PM_{2.5}$, PM_{coarse}, SO_2 and VOC species that were precategorized into the functional groups considered in the CB05 chemistry mechanism.

For the other countries that were completely or partially included in the CNC12 domain, monthly, gridded emissions from EDGAR v5.0 were used at a 0.1° × 0.1° spatial resolution. The EDGAR inventory covered 9 pollutants, i.e., BC, CO, NH_3, NMVOC, NO_X, OC, PM_{10}, $PM_{2.5}$ and SO_2, of 27 activities that are based on IPCC 1996 and 2006 sector codes (see Section S1 of the supplementary material for the sector mapping). All nonshipping anthropogenic emissions were distributed from a monthly to an hourly resolution. The individual temporal patterns for countries and sectors were considered by applying the high-resolution temporal profiles developed by Crippa et al. [63]. For this, the five sectors of the MEIC inventory were mapped to fit EDGAR activities (Section S1). A sector-wise vertical distribution up to 1106 m was carried out by applying the height profiles described in Bieser et al. [64].

To be compatible with the application in CMAQ, NO_X emissions were split into NO and NO_2 at a ratio of 90 to 10 for road traffic and 95 to 5 for all other sectors. Furthermore, NMVOC emissions from EDGAR were split sector-wise according to a profile of The Netherlands Organisation for Applied Scientific Research (TNO) into the functional groups

of the CB05 mechanism. $PM_{2.5}$ splits were applied from the SMOKE for Europe emission model by Bieser et al. [65].

2.2.3. Biogenic Emissions

Emissions from biogenic sources were calculated with the Model of Emissions of Gases and Aerosols from Nature (MEGAN) in version 3 for both model domains [66,67]. MEGAN was driven by the same meteorological data preprocessed for CMAQ (see Section 2.1.3) Vegetation data tables were used unmodified from the official MEGAN resources [68]. SPOT/PROBA V LAI1 from GEOV1 products was chosen as an alternative input for leaf area index (LAI) data in MEGAN [69].

2.2.4. Ship Emissions in Northern Europe

The ship EI for northern Europe was created with the MoSES model using data from the automatic identification system (AIS) that were recorded by the European Maritime Safety Agency (EMSA), which was acquired from the Federal Maritime and Hydrographic Agency of Germany (BSH). The European inventory covered the area between the longitude and latitude ranges −5.00–31.41° and 48.32–68.37°, respectively. The spatial resolution was 0.069° in the x (east–west) and 0.036° in the y (north-south) directions, which corresponded to approximately 4 km. The temporal resolution was hourly. A detailed description of this ship EI and details about the bottom-up methods used for the calculation can be found in Schwarzkopf et al. [37]. To cover the whole computational SC12NSBS domain (Figure 1, left), the ship emission inventory was augmented at the northern and western boundary with data from the Ship Traffic Assessment Model (STEAM) described in detail in Jalkanen et al. [70,71], Johansson et al. [72,73]. The STEAM data were part of the CAMS-GLOB-SHIP dataset (v2.1) and can be downloaded at the Emissions of Atmospheric Compounds and Compilation of Ancillary Data website [74]. The emission inventory of MoSES was scaled up to fit the grid of the STEAM data (regular lon.-lat. with a 0.1° resolution) and then merged.

Table 1 lists the gas and aerosol species included in the ship EIs, together with a reference to the source of the EFs used. NO_X emissions were split into NO and NO_2 in the ratio of 92 to 8 for shipping. NMVOCs were split according to data from the Finnish Meteorological Institute (FMI), which was consistent with the results from CIMAC [75] $PM_{2.5}$ emissions from ships were split with data from the SMOKE for Europe emission model [65]. Finally, the merged data set was fed into the CMAQ model as emission input.

Table 1. Gas and aerosol species included in the ship emission inventories (EIs), with sources of the emission factors (EFs) used.

Pollutant	EF Source
Sulfur dioxide (SO_2)	—
Sulfate (SO_4^{2-})	Schwarzkopf et al. [37]
Water associated with sulfate ($SO_4 \times H_2O$)	Jalkanen et al. [71]
Nitrogen oxides (NO_X)	Zeretzke [76]
Black carbon (BC)	Aulinger et al. [22]
Primary organic aerosols (POAs)	Jalkanen et al. [71]
Mineral ash excl. metal sulphates (MA)	Schwarzkopf et al. [37]
Carbon dioxide (CO_2)	IMO [3]
Carbon monoxide (CO)	IMO [3]
Methane (CH_4)	IMO [3]
Nonmethane volatile organic compounds (NMVOCs)	EMEP/EEA [77]
Dinitrogen oxide (N_2O)	IMO [3]
Particulate matter (PM_{tot})	EMEP/EEA [77]

2.2.5. Ship Emissions in China

The ship EI for China covered the area between the longitude and latitude ranges 133.15–102.09° and 44.47–15.54°, respectively. The AIS data used for this inventory were

obtained through a collaboration with the Shanghai Maritime Department. The ship EI for China generated from these data, had a spatial resolution of 0.039° in the x (east–west) and the y (north–south) directions, corresponding to approximately 4 km. The temporal resolution is hourly. For better comparability of the model results, the same parameters and EFs were used with MoSES for this EI as for the EI of northern Europe (Table 1, see also for details [37]).

The spatial distribution of CO_2 emission fluxes for 2015 in the CNC12 domain and monthly, normalized emission totals for each considered species are illustrated in Figure 2. The monthly variation in ship emissions showed two minima. The first minimum was registered in February during the long public holidays of the Chinese Spring Festival, and the second minimum was seen during the summer months, which corresponded to the summer fishing moratorium. In contrast, higher fishing activities and corresponding emissions were found in spring and autumn. Similar observations were also made by Chen et al. [78] and Fan et al. [79].

For the calculation of ship emissions, 10 ship types were differentiated plus an "Undefined" class, used for ships for which no type information was present. These were Bulk, Cargo and container, Cruise, Fishing, Military, Passenger and Ro-Ro, Pleasurecraft, Tanker, Tug and Other. The annual emissions for 2015 are shown in Table 2 as totals and for the individual ship types. The majority of emissions could be accounted for by freight ships. Hereby, cargo ships, including container and Ro-Ro cargo ships, had the largest share, with an annual average of 38% of SO_2, SO_4 and MA, 45% of NO_X, CO_2, CO, NMVOC, N_2O, BC and POA and 10% of CH_4 and 43% of PM_{tot} emissions. A decreased activity for this ship type was modeled in February and March. Bulk freighters instead accounted for only 1% of SO_2, SO_4 and MA, 14% of CO_2, CO, NO_X and N_2O, 3% of CH_4, 9% of NMVOC and BC, 11% POA and 5% PM_{tot} emissions. The share of tankers, the last type of freight ships considered, was 7% of the emissions of SO_2, SO_4, MA and PM_{tot}. They also accounted for 11% of the emissions of NO_X, CO_2, CO and N_2O, 80% of CH_4 and 9% of NMVOC, BC and POA. In total, freight ships accounted for approximately 50–70% of ship emissions and for almost all methane emissions. The emission share of fishing vessels in the model domain was 5% of SO_2, SO_4 and MA, 3% of NO_X, CO_2, CO, NMVOC, N_2O, BC, POA and PM_{tot} and 1% of CH_4 emissions. A seasonality for emissions from fishing vessels was observed, with increased emissions in April and May and October. An explanation for this was the summer fishing ban in the South China Sea enforced since 1999 (https://www.fao.org/fishery/en/facp/chn, last accessed: 14 December 2021). This resulted in a decrease in CO_2 emissions to 1% in June, which increased to 5% during peak periods. Tugs and passenger ships accounted for only 2–3% of the emissions of the species considered. Cruise ships, military ships and pleasurecrafts accounted for a negligible share of all emissions species considered, with less than 1%. In this context, it should be noted that AIS is not a reliable source for tracking military vessels. Ships of other types, grouped under the type "Other" (e.g, dredging or drilling ships, patrol or research vessels) accounted for 17% of SO_2, SO_4, MA and PM_{tot}, 9% of NO_X, CO, N_2O and POA, 8% of CO_2, 2% of CH_4 and 13% NMVOC and BC emissions. Ships for which no type could be determined due to missing data were assigned the type "Undefined". Various assumptions had to be made for this type, which usually included estimations of the engine power and fuel type. When vessel size information was not available, "Undefined" ships were considered small, and an approximated gross tonnage of 500 was found to be plausible [37]. This result was supported by the two assumptions that large and commercial vessels are considered more reliable in transmitting information via AIS and that the available vessel characteristics databases are more reliable for larger vessels.

In the CNC12 domain, undefined ships are responsible for approximately 26% of SO_2, SO_4 and MA, 14% of NO_X and CO_2, 13% of CO, NMVOC and N_2O, 3% of CH_4 and 16% of PM_{tot}, POA and BC emissions. Numerically, nearly 57% of the vessels had to be classified as "Undefined"; no information on installed main engine power was available for nearly 92% of them. This corresponds to a share of 67% of all vessels for which the installed main

engine power had to be estimated. Similar findings were made by Zhang et al. [80] for the PRD, where unidentified ships accounted for 49% of CO_2 emissions. This introduces an uncertainty to the calculated emissions due to the estimations that had to be made. In comparison, 11% of undefined ships by number were found in the European EI. Estimations about the main engine power had to be made for more than 56% of ships and for 31% of the total on ships installed main engine power.

In both regions, oil-based residual and distillate fuels are predominant, being used by more than 99% of registered vessels. However, in China, 65% of vessels were found using residual fuels, compared to 37% in Europe. The vast majority of the remaining ships use distillate fuels. The more frequent application of residual fuels is, in addition to the differing legal regulations, responsible for higher SO_X and particle emissions in China.

Of the more than 110,000 of different vessels registered in China in 2015 and of the nearly 22,000 registered in Europe, 4090 vessels were found in both regions. Most of them, 95%, were freight ships, with a gross tonnage over 5000. This was plausible, as larger ships are usually deployed for this long voyage. They were distributed among the ship types considered: 38% bulk freighters, 35% cargo and container ships, 23% tankers, 2% other ships. The remaining ship types make up less than 1%.

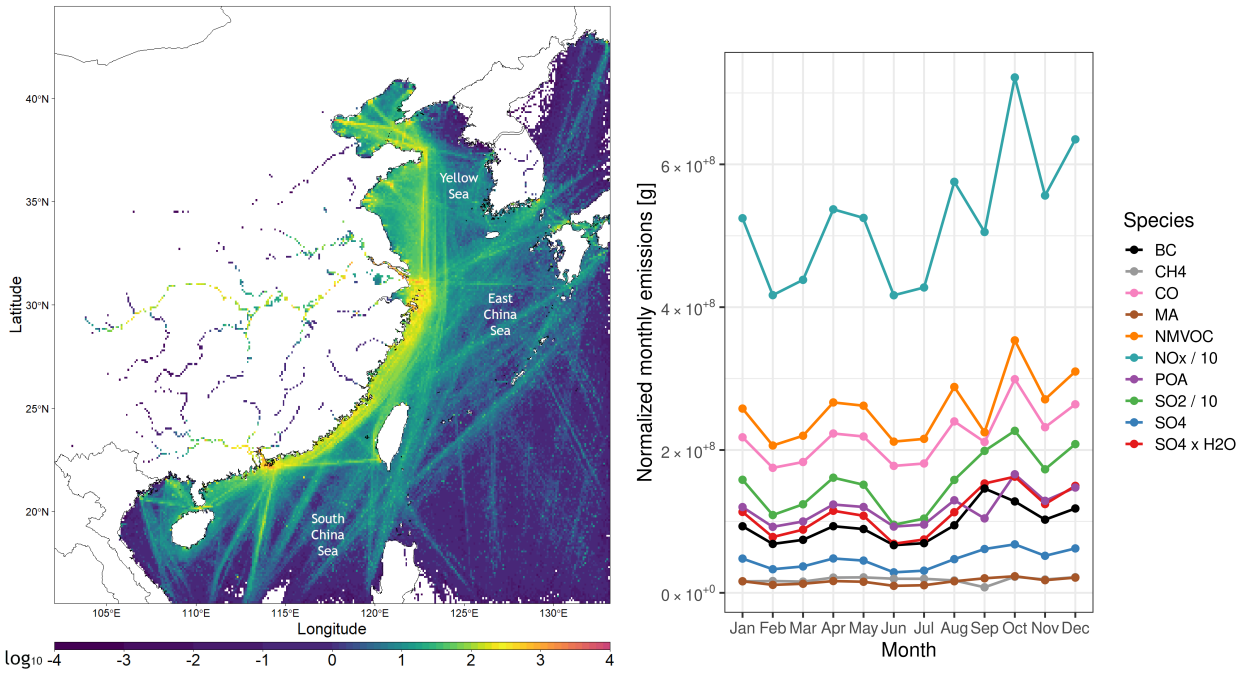

Figure 2. Calculated CO_2 emission flux in $g \cdot m^{-2} \cdot year^{-1}$ plotted with a logarithmic scale for the Chinese domain 2015. The spatial resolution is approximately $4 \times 4\,km^2$ (**left**). Monthly emissions of black carbon (BC), CH_4, CO, mineral ash (MA), nonmethane volatile organic compounds (NMVOCs), NO_X, primary organic aerosols (POAs), SO_2, SO_4 and $SO_4 \times H_2O$ in 2015, normalized to one day (**right**). Values of NO_X and SO_2 were divided by 10 to fit the scale.

Table 2. Modeled ship emissions in Gg · year^{-1} for China in 2015 in total and for each individual ship type.

Ship Type	SO_2	SO_4	SO_4 xH_2O	NO_X	CO_2	CO	CH_4	NM VOC	N_2O	BC	MA	POA	PM_{tot}
All	486.55	14.38	11.22	1678.98	85,325.01	70.3	5.97	21.93	4.36	29.94	4.98	39.87	89.34
Bulk	6.43	0.13	0.10	219.43	12,144.84	9.95	0.20	1.95	0.60	2.81	0.07	4.53	6.80
Cargo	181.93	5.28	4.12	750.25	39,012.88	31.12	0.58	10.22	1.94	13.66	1.86	17.98	38.18
Cruise	0.63	0.02	0.02	8.33	363.08	0.34	0.01	0.06	0.02	0.10	0.01	0.18	0.29
Fishing	26.17	0.77	0.60	51.23	2445.1	2.01	0.03	0.67	0.13	1.03	0.27	1.42	3.68
Military	0.37	0.01	0.01	0.94	43.38	0.04	0.00	0.02	0.00	0.02	0.00	0.02	0.05
Passenger	10.69	0.35	0.27	45.98	1925.97	1.82	0.03	0.59	0.12	0.74	0.11	0.99	2.19
Pleasurec.	1.11	0.03	0.02	2.17	103.08	0.09	0.00	0.05	0.01	0.05	0.01	0.05	0.15
Tanker	31.89	0.99	0.77	177.59	8978.86	8.43	4.83	1.88	0.48	2.54	0.33	3.60	7.33
Tug	15.91	0.49	0.38	27.90	1600.8	1.36	0.03	0.59	0.09	0.74	0.16	0.85	2.33
Other	81.46	2.45	1.91	150.52	6679.75	5.89	0.10	2.94	0.38	3.54	0.83	3.78	11.13
Undef.	129.96	3.85	3.00	244.63	12,027.27	9.26	0.16	2.96	0.60	4.70	1.33	6.46	17.22

3. Assessment of the Model Performance

To assess the reliability and performance of the model results for the European SC12NSBS and Chinese CNC12 domains, they were compared with publicly available air quality data from the European Environment Agency (EEA) and the Chinese authorities. The data for Europe were acquired from the Air Quality e-Reporting (AQER) repository, which contains data from 2013 onwards [81]. The data for China were acquired from the China National Environment Monitoring Centre (http://www.cnemc.cn, last accessed: 27 April 2022).

Since the focus was on the influence of ship emissions, measurement data from monitoring stations in coastal regions near the major shipping routes were evaluated. Note that a point measurement at the station site and an average concentration in a 12 × 12 km grid cell enclosing the station were compared. Therefore, the measured concentrations may not be fully representative of the grid cell, as the resolution of the regional model does not allow for the consideration of small-scale measurement conditions and effects near the station. Although the uncertainties of this method are hard to estimate, it can be seen as a performance indicator for the model.

A comparison of the concentration time series was performed (for NO_2 and SO_2, emissions were included in the comparison), and statistical quantifiers were calculated from the hourly concentrations for each pollutant. These include the geometric mean for all stations, two arithmetic mean values calculated using only positive or negative normalized mean biases (NMB_{pos}, NMB_{neg}) and the arithmetic mean of the Spearman correlation coefficients. Only stations with data availability greater than 60% of hourly measurements for 2015 were considered for comparison. A total of 29 stations in the SC12NSBS domain and 20 stations in the CNC12 domain were considered (their locations are shown in Figure 1). A comparison of the modeled "base" case concentrations with the measured data is shown for 6 selected stations for each domain. These include statistical quantifiers calculated with data from all stations (Table 3). The comparison data of all stations are shown in Tables A1 and A2. For station-specific NMBs and correlation coefficients for the modeled "base" and "no ships" case, refer to Section S2 of the supplementary material. A high correlation coefficient was an indicator of the representativeness of the time profiles used for the concentration patterns at the monitoring station. A correlation was considered for a coefficient greater than or equal to 0.5. The correlation was considered "good" if the coefficient was equal to or greater than 0.7.

Table 3. Comparison of modeled NO_2, SO_2, O_3 8-h mean and $PM_{2.5}$ concentrations of the modeled "base" case for selected stations in $\mu g \cdot m^{-3}$ with measurements in the SC12NSBS domain. Based on all 29 considered stations in Europe, the mean correlation coefficient (Mean Corr.) and two values, calculated as the mean of either positive or negative normalized mean biases are shown (NMB_{pos}, NMB_{neg}). For the latter two values, the number of stations used for the calculation is given in parentheses.

	NO_2		SO_2		O_3 8-h Mean		$PM_{2.5}$	
Station	**$Mean_{model}$**	**$Mean_{meas}$**	**$Mean_{model}$**	**$Mean_{meas}$**	**$Mean_{model}$**	**$Mean_{meas}$**	**$Mean_{model}$**	**$Mean_{meas}$**
Narberth	1.60	1.63	0.37	0.68	75.12	61.09	—	—
Lull. Heath	4.44	4.79	0.28	0.95	73.98	53.61	—	—
De Zilk	12.99	9.83	0.73	0.95	48.49	42.27	9.73	6.61
Ostf. Inseln	3.43	6.39	0.14	0.40	72.08	55.72	—	—
Zingst	2.95	3.73	0.21	0.39	72.69	57.10	—	—
Helsinki	5.90	14.01	1.00	0.61	58.39	44.94	4.84	4.22
Mean NMB_{pos}	0.398 (1)		0.365 (10)		0.27 (28)		0.164 (9)	
Mean NMB_{neg}	−0.38 (28)		−0.266 (6)		n.a.(0)		−0.03 (2)	
Mean Corr.	0.617		0.279		0.659		0.377	

All of the 29 stations in the SC12NSBS domain in Europe were background monitoring stations in less densely populated locations, e.g., suburban or rural stations were preferred in the selection. NO_2 concentrations were often underpredicted by the model, indicated by 28 of 29 stations having a negative NMB. For 6 of the 29 stations a correlation coefficient of 0.7 or greater was found. For 26 stations, the coefficient was greater than or equal to 0.5. In general, the NMB was higher for stations where lower concentrations were modeled. When comparing the "base" with the "no ships" case, lower concentrations were found at all stations, which highlights the importance of including ship emissions in the model. Consequently, a higher absolute NMB was calculated, indicating a poorer agreement between the "no ships" and the measurements. This was consistent with the assumption that shipping is an important source of air pollution for many of these stations because they were located near major shipping routes. Considering the correlation, differences were not so clear since the disparities between the "base" and "no ships" cases were small.

In the SC12NSBS domain, SO_2 concentrations were generally low at the stations considered, mostly below $1\ \mu g \cdot m^{-3}$. In comparison to the measurements, the modeled SO_2 concentrations were often overestimated, as 10 of the 16 stations had an NMB greater than zero. A correlation coefficient greater than 0.5 was calculated for only one station. The low correlation could be explained by the overall low SO_2 concentrations, which are both difficult to measure and model. The correlation differences between the "base" and "no ships" cases were generally small.

The distinct diurnal concentration changes and seasonal trends of the O_3 8-h mean were well represented in the model results, as shown by correlations greater than 0.5 for all 28 stations. For 9 stations, the correlation was greater than 0.7. The average NMB of 0.27 indicated that concentrations at all 28 stations were systematically overestimated. This overestimation was most concise in spring and autumn. Furthermore, large daily fluctuations were often not captured well by the model. In general, the correlation was better for the "base" case than for the "no ships" case. The performance gain of the model by including ship emissions was small for most stations. However, for stations close to the port cluster of Rotterdam and Antwerp, i.e., Schoten, De Zilk and Den Haag, the performance gain was significant. The observed ozone reduction by ship exhausts in this region is also visible in concentration patterns, which are shown and discussed later in Section 4.3.

Of the 29 stations in total, $PM_{2.5}$ was only measured at 11 sites in The Netherlands, Belgium, England and Finland. According to the NMB, the modeled concentrations were mostly overestimated. For two stations, a correlation equal to or greater than 0.5 was calculated; for none, a correlation equal to or greater than 0.7. The low correlation was explained in terms of the complex nature of ambient $PM_{2.5}$ concentrations. The chemical and physical transformations that generate particulate matter, and that particles themselves undergo mostly depend on location-specific parameters. Local events can generate high fluctuations in hourly measurements, which are difficult to reproduce with a regional model. However, the correlation coefficient increased at all regarded stations by the inclusion of ship emissions. The NMB decreased for some cases due to an overestimation of the concentrations.

The 20 stations in the CNC12 domain in China are located in or close to large coastal cities (Table 4).

Table 4. Comparison of modeled NO_2, SO_2, O_3 8-h mean and $PM_{2.5}$ concentrations of the modeled "base" case for selected stations in $\mu g \cdot m^{-3}$ with measurements in the CNC12 domain. Based on all 20 considered stations in China, the mean correlation coefficient (Mean Corr.) and two values, calculated as the mean either from positive or negative normalized mean biases are shown (NMB_{pos}, NMB_{neg}). For the latter two values, the number of stations used for the calculation is given in parentheses.

	NO_2		**SO_2**		**O_3 8-h Mean**		$PM_{2.5}$	
Station	**$Mean_{model}$**	**$Mean_{meas}$**	**$Mean_{model}$**	**$Mean_{meas}$**	**$Mean_{model}$**	**$Mean_{meas}$**	**$Mean_{model}$**	**$Mean_{meas}$**
Tianjin	56.95	33.53	29.83	19.00	4.32	29.99	59.93	50.52
Lianyungang	15.05	24.31	4.75	22.07	57.19	60.35	42.26	39.82
Nantong	36.79	30.45	11.84	23.50	37.06	62.88	42.19	45.28
Ningbo	44.97	37.27	16.06	14.36	36.73	50.95	37.51	35.30
Shantou	15.01	16.98	6.05	11.64	78.48	61.95	42.11	28.22
Zhuhai	14.25	23.30	5.03	7.03	79.18	51.72	45.85	23.98
Mean, NMB_{pos}	0.402 (12)		0.512 (9)		0.544 (18)		0.439 (17)	
Mean, NMB_{neg}	−0.283 (8)		−0.38 (11)		−0.1 (2)		−0.06 (3)	
Mean Corr.	0.477		0.398		0.628		0.408	

NO_2 concentrations were overestimated at 12 of the 20 stations, but at 9 of these 12 stations, the NMB was only small (≤ 0.1). An underprediction was found for 8 stations, of which 7 had an NMB lower than −0.1. No general systematic was found for this observation. An analysis of the NO_2 emissions that were used as input for the model run leads to manifold reasons. For stations bordering the Bohai Sea, emissions were either too high or too low. In Jiangsu Province, summer and winter trends were not well captured. NO_X emissions were also too high for the stations in Shanghai and Ningbo; in the case of Shanghai, this may be related to the location of the monitoring station, which is on the Huangpu River, while the corresponding model cell covers a large part of the urban center. A comparison of the model results with the measurements in the PRD showed that the diurnal trend was more pronounced in the model than in the measurements. At the three southernmost stations, emissions were found to be too low. A correlation coefficient greater than 0.5 was found for 8 stations; no station had a correlation greater or equal 0.7. The low correlation might be explained by the urban environments in which most stations are located, which has a large influence on the hourly concentration patterns. Nevertheless, the main concentration features could be reproduced for most stations with the applied time profiles, although some concentration peaks were slightly shifted in time.

In general, the measured and modeled SO_2 concentrations at stations in China were much higher than those in Europe. The model underestimated the concentrations of SO_2 at 11 and overestimated them at the other 9 stations. The correlation coefficient was greater

than or equal to 0.5 for 7 stations and was not greater than or equal to 0.7 for any station. In contrast to Europe, better correlations were calculated, which is probably related to the higher SO_2 concentrations. An examination of the emissions at the measurement sites suggested that SO_2 emissions were mainly too high at station sites in the YRD or PRD. Too low emissions were frequently found at northern stations, e.g., Huludao, Qinhuangdao, Lianyungang and Yancheng.

Similar to Europe, the diurnal ozone fluctuations were well modeled, but concentrations were overestimated at 17 of 20 stations. However, the correlations were greater than or equal to 0.5 at 16 stations and greater than or equal to 0.7 at 7 stations. In general, the correlation coefficients in China were higher for the northern stations than for the southern stations. In the north, overestimations were observed mainly during summer, while this trend was reversed in the south, which is presumably related to the regionally different climate zones. While the strong daily O_3 fluctuations in Europe were often underestimated, the results for China were in better agreement. The largest improvements from the inclusion of ship emissions were found in southern China, e.g., Quanzhou, Fuzhou and Wenzhou. In the large port clusters in the YRD or PRD, the impact of ships on ozone concentrations was small.

Compared to the measurement data, the modeled $PM_{2.5}$ concentrations were overestimated. A correlation coefficient greater than or equal to 0.5 was calculated for 7 stations all located in the northern part of the domain, i.e., Wenzhou, and at stations further north with a steady increase in correlation up to 0.69 at Qinhuangdao. Additionally, a small NMB was calculated for these stations. In southern China, the model performance for $PM_{2.5}$ was worse. While the mean of the 10 stations, including Fuzhou and those farther south, had an average NMB of 0.66, the average NMB for Wenzhou and the 10 stations further north was 0.11. Based on this observation, it is assumed that the model performs better in the calculation of $PM_{2.5}$ concentrations for the temperate climate zone.

In summary, the model performance was found to be satisfactory in both domains; however, different conclusions were drawn for Europe and China. The predominantly underestimated NO_2 concentrations in Europe, although with good correlations, suggest a systematic bias. The under- and overestimates in China and the moderate correlations indicate inconsistencies in the emission inventory and occasional difficulties of the model in describing NO_2 concentrations under the local meteorological conditions and atmospheric background. The better performance and correlation for SO_2 in China is related to the difficulties in modeling and measuring the low concentrations that occur in Europe. The pronounced diurnal trends in ozone concentrations were well captured in both domains, as reflected by high correlation coefficients, but a systematic overprediction of ozone concentrations was found for both regions. Concentrations of $PM_{2.5}$ were mostly overpredicted in both domains. Furthermore, it is noteworthy that in China the accuracy for modeled $PM_{2.5}$ concentrations increased at sites further north, which might be related to the temperate climate. However, caution must be exercised in interpreting these observations, as consideration of the immediate environment of the measurement site and small-scale effects is only limited to 12×12 km resolved model runs. It should also be emphasized that the stations selected for Europe are mostly nonurban background stations, while most of the monitoring stations in China are located in or near major cities. Moreover, differences in the methodologies and sources that were used to create the nonshipping anthropogenic EIs are hardly avoidable. For the CNC12 domain, a second model run was carried out, in which anthropogenic, nonshipping emissions for China were used from the EDGAR instead of the MEIC inventory. The EDGAR inventory has a higher resolution of 0.1°, compared to 0.25° in MEIC. However, the results obtained with EDGAR showed higher overestimations, compared to MEIC. This was especially the case for NO_2 and O_3. Thus, it was decided that the MEIC inventory would be more reliable for China.

4. Results and Discussion

Pollutants from ship exhausts can be transported over land by onshore winds to degrade air quality in populated areas. During this transport, a portion is removed from the atmosphere by wet and dry deposition processes. Furthermore, chemical reactions are responsible for the formation of secondary pollutants and particulates. For the latter, ammonia emissions from agriculture play a significant role. Rates for the relevant chemical transformations generally increase with temperature. In contrast, nucleation and coagulation of the particulation processes are facilitated at lower temperatures. All of these processes are considered within CMAQ and result in concentration patterns that are discussed and compared for northern Europe and eastern China.

In general, primary pollutants from shipping had the largest impact close to densely shipped routes (e.g., the Yangtze River, the English Channel or the southern North Sea) and in the vicinity of large port clusters (e.g., in the YRD, PRD or Rotterdam/Antwerp/Amsterdam). In Europe, prevailing southwesterly winds transported pollutants towards populated areas. In China, prevailing south and southeasterly winds transported ship emissions onto coastal regions, especially over the flat terrain of the Lower Yangtze Plain (LYP) and North China Plain (NCP). Meteorological conditions proved to be more important for an understanding of the seasonal patterns of ship pollutant concentrations than fluctuations in ship traffic [82]. In particular, the East Asian monsoon is a dominant factor for emissions from a marine environment. Secondary pollutants generally have a higher atmospheric lifetime and can thus be encountered farther away from marine shipping lanes. They were found to have a higher impact on extended coastal regions in both domains.

For an interpretation of the results and an assessment of the impact ship emissions have on air quality, total regional pollutant concentrations must be considered, as well as the contribution from ships only. This was done for the pollutant species NO_2 (Section 4.1), SO_2 (Section 4.2), ozone (Section 4.3), $PM_{2.5}$ (Section 4.4) and the main components of PM2.5 from shipping, ammonium (Section 4.4.1), sulfate (Section 4.4.2) and nitrate (Section 4.4.3). The contribution of shipping was determined by the zero-out method, i.e., by subtracting the results of a model run with omitted ship emissions from a model run that considers all emission sources. All concentration fields shown in the following are annual averages, unless otherwise specified. Seasonally averaged concentration fields are found in Section S3 of the supplementary material to avoid disrupting the reading flow by their large numbers. All concentrations are given in $\mu g \cdot m^{-3}$. The contribution of shipping to the total pollutant concentrations is shown as a percentage.

4.1. NO_2

Nitrogen dioxide emissions are mainly the result of nitrogen oxidation during combustion processes. NO_2 plays an important role in the formation of ground-level ozone (see Section 4.3) and as a precursor of PM (Sections 4.4 and 4.4.3).

In Europe, annual average concentrations of 15–20 $\mu g \cdot m^{-3}$ were modeled near major cities and industrialized areas, e.g., London, Paris, Prague, the Rhine-Ruhr or Rhine-Main metropolitan regions. The overall highest NO_2 concentrations of 30–35 $\mu g \cdot m^{-3}$ were modeled in the area of the Rotterdam/Antwerp/Amsterdam port cluster (Figure 3a).

In the coastal regions of mainland Europe bordering the North Sea and the southeastern coast of the United Kingdom, 1–4 $\mu g \cdot m^{-3}$ NO_2 could be attributed to shipping, even up to 100–150 km from the coastline (Figure 3b). The contribution of shipping to total NO_2 varied between 20 and 40% in these regions. In ports, almost 50% of NO_2 could be attributed to ships (Figure 3c). Due to higher shipping activities in spring and summer, slightly higher concentrations were modeled for these seasons (Figure S2). In winter and autumn, the contribution of shipping to total NO_2 was lower as NO_2 emissions from residential heating increased and shipping activity decreased (Figure S3).

In China, the concentrations of NO_2 were mostly in the range of 20 to 50 $\mu g \cdot m^{-3}$. In densely populated regions, large cities and heavily industrialized areas, NO_2 concentrations

reached 60 to 90 $\mu g \cdot m^{-3}$, e.g., in Jiangsu, Tianjin, Hebei, the PRD, Shanghai, Beijing and the Sichuan Basin (Figure 3d).

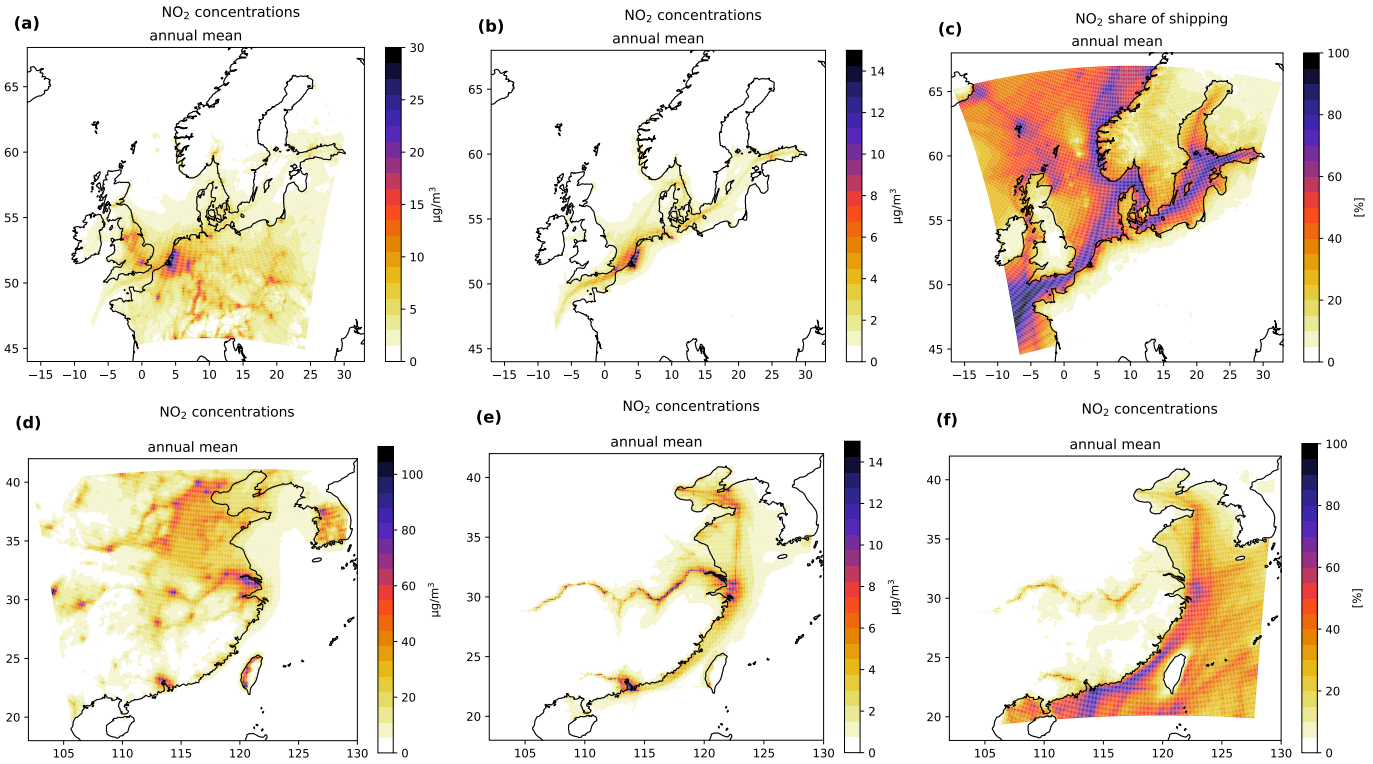

Figure 3. Annual averages of NO_2 concentrations in the SC12NSBS domain in Europe (**a**–**c**) and in the CNC12 domain in China (**d**–**f**). NO_2 concentrations [$\mu g \cdot m^{-3}$] from all emission sources are shown in (**a**,**d**), from shipping only in (**b**,**e**) and the share of NO_2 concentrations from shipping on total NO_2 concentrations [%] is shown in (**c**,**f**).

The impact of shipping on regional NO_2 concentrations was most evident in the YRD, PRD, the associated rivers, the LYP and NCP. NO_2 concentrations were in the range of 2 to 8 $\mu g \cdot m^{-3}$ but could locally increase up to 13 $\mu g \cdot m^{-3}$ (Figure 3e). Vessel traffic was found to be responsible for 10–20% of the NO_2 concentrations in the major port clusters and the LYP and NCP. The highest contribution of up to 50% to the total NO_2 concentrations was modeled in parts of the Yangtze and Pearl Rivers (Figure 3f). In large parts of the Chinese coast, onshore pollutant transport and the impact of NO_2 by ships were small. In autumn and particularly in winter, higher ship-induced NO_2 concentrations and an extended dispersion were modeled, especially close to the Yangtze River (Figures 4a and S6). This was consistent with the results of Shah et al. [83] and could be explained by the longer lifetimes of NO_X. High NO_2 and SO_2 concentrations from other sectors created oxidant-limited conditions during these seasons that reduced the conversion rate for NO_2-depleting reactions, such as conversion to nitrate or nitric acid. Additionally, atmospheric oxidants such as ozone or hydroxyl radicals were less readily formed in winter due to lower solar irradiance. Furthermore, the frequent northerly and northwesterly winds during winter were able to transport more pollutants from shipping and other sectors from coastal regions to the open ocean. Combined with the reduced shipping activity, this explained the lower contribution of ships to NO_2 in coastal areas during this season. The relatively low concentrations over the Yellow Sea in autumn could be related to dilution by cold air currents from the northeast [82].

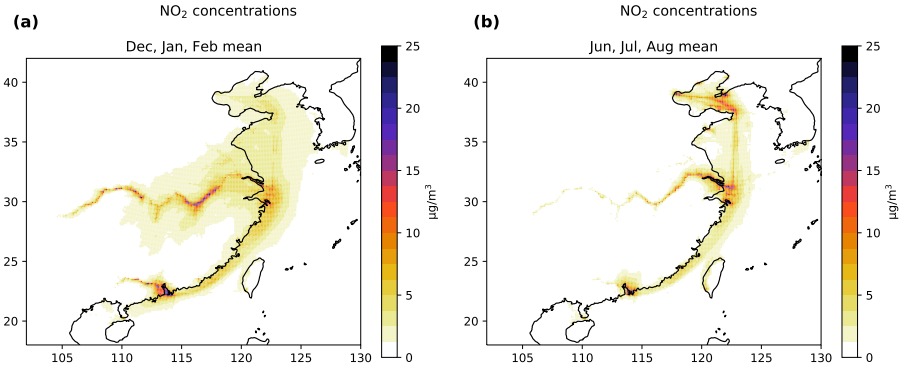

Figure 4. Seasonal averages of NO_2 concentrations [$\mu g \cdot m^{-3}$] from shipping in the CNC12 domain in China for winter (**a**) and summer (**b**).

When the two regions were compared, approximately 2.5 times higher NO_2 concentrations were found in China. With only slightly higher ship-related NO_2 concentrations in China, the relative contribution of NO_2 from ships was 30–40% and thus higher in European ports. Furthermore, NO_2 concentrations from ships showed little seasonality in Europe, with slightly higher concentrations in spring and summer. In China, reduced NO_2 concentrations were modeled in spring and summer, especially in the southern coastal regions (Figures 4b and S5). Higher deposition rates during the summer monsoon were responsible for this observation. Furthermore, high overall NO_2 concentrations in China during winter resulted in increased transport and a further dispersion of NO_2 from shipping in inland areas (Figure 4b).

4.2. SO_2

Sulfur dioxide emissions are mainly generated by the combustion of fossil fuels. Similar to NO_2, it can form secondary aerosols by oxidation, e.g., sulfate (Sections 4.4 and 4.4.2).

In Europe, SO_2 was emitted mainly from coal power plants, e.g., in the Rhine-Ruhr region in Germany or in the Polish provinces of Lodz, Opole and Silesan. Elevated concentrations of 12.5 $\mu g \cdot m^{-3}$ were common near these coal power plants, and concentrations up to 4 $\mu g \cdot m^{-3}$ were modeled in large parts of Poland (Figure 5a). In winter and autumn, SO_2 concentrations were higher due to residential heating (Figure S7).

Since an SECA was introduced in the North Sea and Baltic Sea in early 2015, SO_2 from shipping has become less important as an air pollutant. Nevertheless, small contributions of less than 0.3 $\mu g \cdot m^{-3}$ (15% of total SO_2) were modeled in the vicinity of the ports of Rotterdam, Amsterdam, Antwerp and Hamburg. From outside of the SECA, SO_2 concentrations of similar magnitude were transported from the major shipping routes to the coastal regions of Brittany (40%). Furthermore, concentrations of up to 0.8 $\mu g \cdot m^{-3}$ (50–70%) were modeled in port cities on the east coast of Ireland and the west coast of the United Kingdom (Figure 5d).

In 2015, 64% of the Chinese domestic energy consumption was produced using coal power plants (26% in Europe) [84,85]). This difference was reflected in higher atmospheric SO_2 concentrations (Figure 5d). In densely populated and industrialized regions, annual averages of 30 $\mu g \cdot m^{-3}$ were modeled with local concentration peaks of up to 100 $\mu g \cdot m^{-3}$. Similar to NO_2, ship traffic contributed the most to SO_2 in the major port clusters in the YRD, PRD and along the Yangtze River, with concentrations ranging from 4 to 8 $\mu g \cdot m^{-3}$ (30–40%). SO_2 concentrations of 1 to 3 $\mu g \cdot m^{-3}$ (10–20%) were modeled along large parts of the coastline (Figure 5e,f). The seasonal patterns of SO_2 were similar to those of NO_2. Concentrations were higher in winter and autumn, especially in the YRD and PRD port clusters and along navigated rivers (Figure S11). It is assumed that, similar to NO_2, chemical conversion and deposition of SO_2 from shipping was inhibited due to high SO_2 emissions from other sectors.

When comparing the two regions, atmospheric SO_2 concentrations in China were found to be approximately 6 times those in Europe. For similar reasons as for NO_2, reverse seasonal trends between the two regions were also modeled for SO_2.

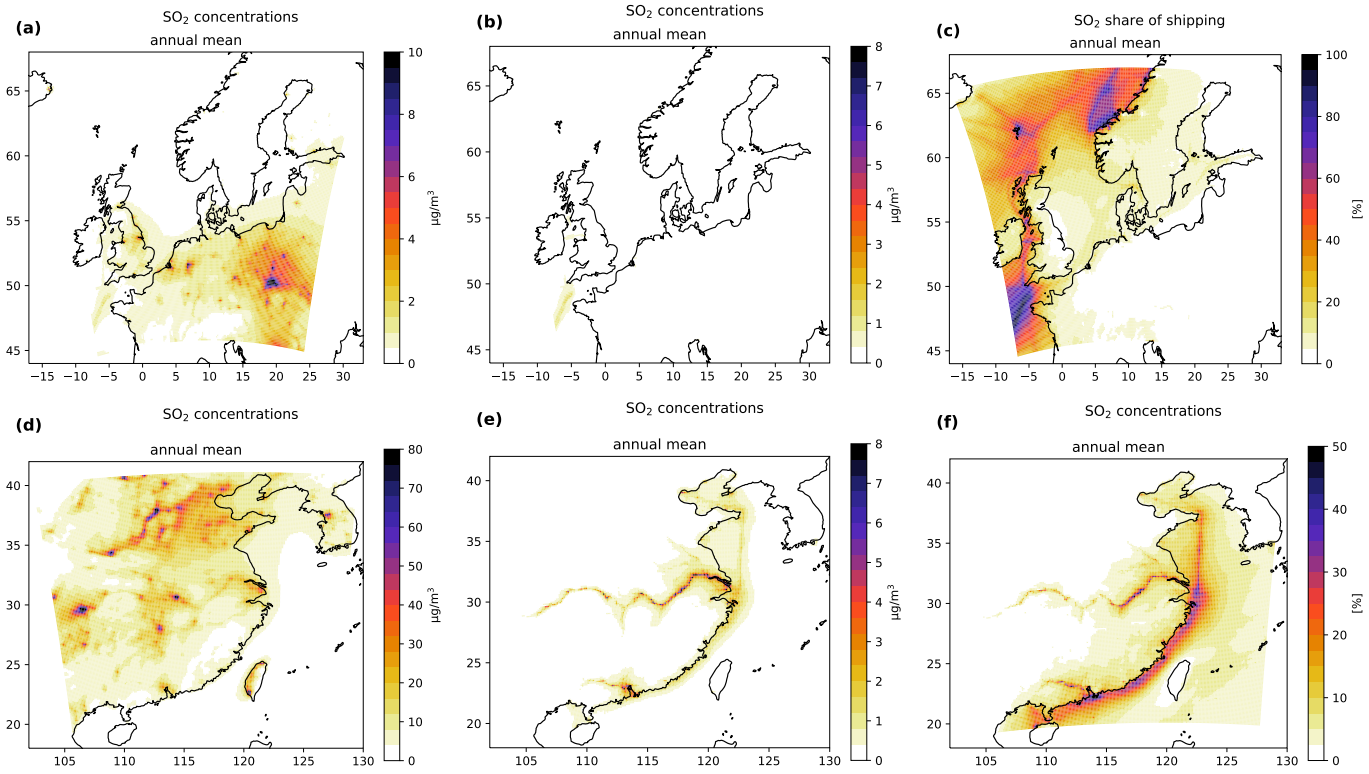

Figure 5. Annual averages of SO_2 concentrations in the SC12NSBS domain in Europe (**a**–**c**) and in the CNC12 domain in China (**d**–**f**). SO_2 concentrations [$\mu g \cdot m^{-3}$] from all emission sources are shown in (**a**,**d**), from shipping only in (**b**,**e**) and the share of SO_2 concentrations from shipping on total SO_2 concentrations [%] is shown in (**c**,**f**).

4.3. Ozone

Tropospheric ozone is known to be harmful to the respiratory tract and is also a potent greenhouse gas [86,87]. O_3 is a photochemical product for which formation solar radiation is the most important factor. However, concentrations of tropospheric ozone are also controlled by the availability of reaction partners, such as NO_X and VOCs. For this reason, high VOC/NO_X ratios can produce NO_X-limited conditions that favor ozone formation and usually occur in rural areas. Vice versa, low VOC/NO_X ratios and VOC-limited conditions are common in urban centers and promote O_3 titration. By this means, ship emissions that contain NO_X and VOCs can have a significant influence on regional ozone concentrations. With respect to the comparison with measurements in Section 3, it must be noted that ozone concentrations were systematically overestimated in both domains.

In Europe, annual averages of 8-hour max. ozone concentrations over land were modeled in the range of 75 to 90 $\mu g \cdot m^{-3}$ (Figure 6a). Due to high cloud coverage in Europe during the summer months of 2015, especially over the North Sea, the United Kingdom and the Scandinavian countries, the modeled O_3 concentrations were lower for summer than spring (Figure S13). However, this result needs to be interpreted with care, as the ozone overestimation was found to be higher in spring than in summer.

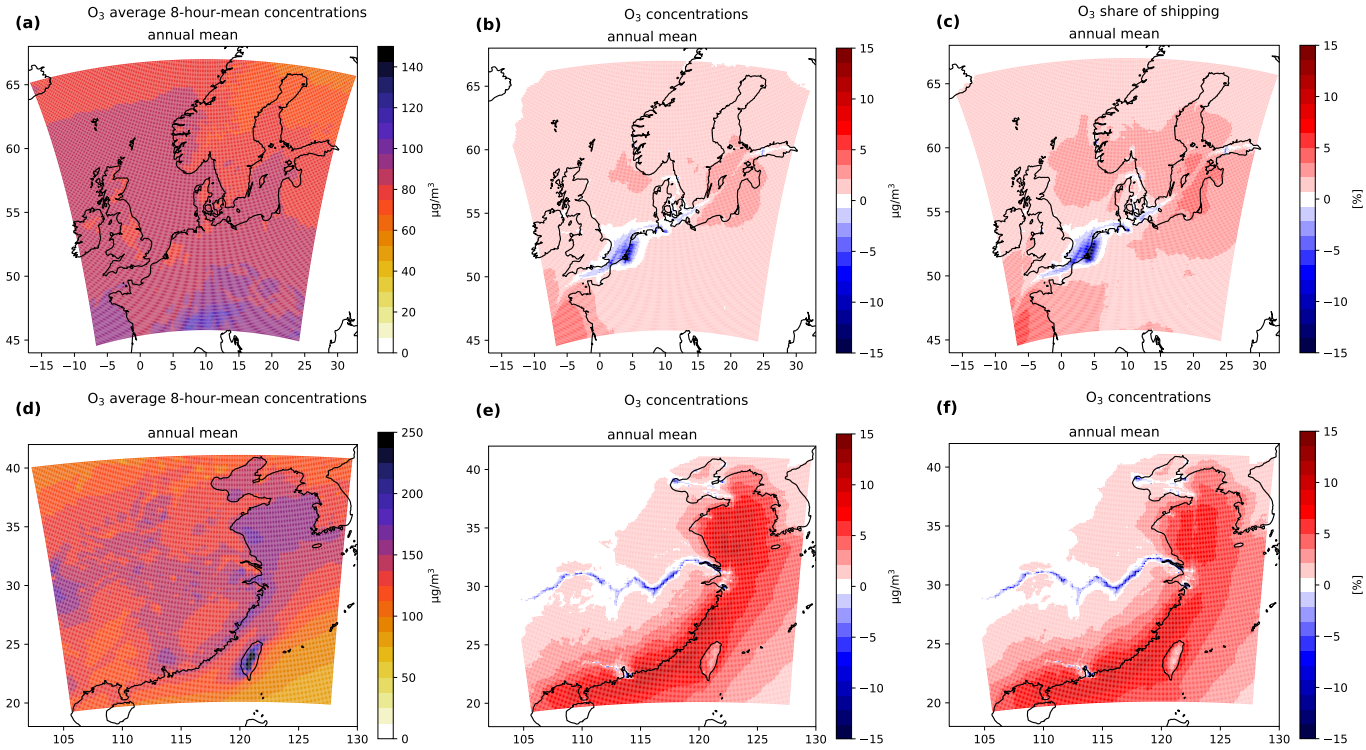

Figure 6. Annual averages of O_3 concentrations in the SC12NSBS domain for Europe (**a**–**c**) and in the CNC12 domain for China (**d**–**f**). Annual averages of 8-hour max. O_3 concentrations [$\mu g \cdot m^{-3}$] from all emission sources are shown in (**a**,**d**), annual averages from shipping only in (**b**,**e**) and the share of O_3 concentrations from shipping on total O_3 concentrations [%] is shown in (**c**,**f**).

Due to high NO_X emissions from shipping and VOC-limited conditions in the area of the harbors of Rotterdam, Antwerp and Hamburg, O_3 concentrations were reduced to approximately 70–80 $\mu g \cdot m^{-3}$ by NO_X-promoted ozone decomposition. This corresponded to an ozone reduction of 10 to 15 $\mu g \cdot m^{-3}$ and a relative reduction of 10 to 15% (Figure 6b,c, illustrated ozone concentrations here represent annual averages instead of averages of the O_3 8-h max.). In other areas of the SC12NSBS domain, ship emissions increased ozone by 1–3 $\mu g \cdot m^{-3}$ (1–3%). The reduction potential was stronger in winter when the solar irradiation was lower (Figure 7a). During summer, a ship-related increase in ozone concentrations by 4 to 8 $\mu g \cdot m^{-3}$ (5–10%) was modeled in Denmark, southern Sweden, Norway and northern Germany, as well as in coastal regions bordering the Baltic Sea and the English Channel (Figures 7b, S14 and S15).

In China, average values of 8-h max. ozone concentrations were modeled between 140 and 150 $\mu g \cdot m^{-3}$. Values were lower in the southern- and northernmost coastal regions, 100–120 $\mu g \cdot m^{-3}$ (Figure 6d). Regarding the seasonality of O_3, different factors had to be considered for mainland China. While in the winter radiation was lower, especially in the northeast, high NO_X emissions from residential heating promoted ozone decomposition. Furthermore, an increased aerosol load was able to take up gaseous precursors relevant for ozone formation [88]. Consequently, O_3 concentrations were very low (e.g., in the LYP and NCP during winter, often less than 50 $\mu g \cdot m^{-3}$).

In China, an ozone reduction from ship emissions of 5–15 $\mu g \cdot m^{-3}$ could mainly be observed along the Yangtze River. As in Europe, the reason for this was a smaller VOC/NO_X ratio, which decreased through ship emissions. At the large port cluster in the YRD and PRD, VOC-limited conditions were plausible; however, the impact of NO_X from ships on ozone degradation was small. An explanation for this was the low relative contributions of ships to the total NO_2 concentrations, which were lower than, for example, in Rotterdam/Antwerp. This was also consistent with the results in Section 3, which indicated that the inclusion of ship emissions has little effect on ozone concentrations in

the YRD and PRD. Increased ozone concentrations due to ship emissions were found along the southern coastline by 4–8 $\mu g \cdot m^{-3}$ (5–8%) and by approximately 2–3 $\mu g \cdot m^{-3}$ along the northern coastline (Figure 6e,f)). Here, it was plausible that ozone whose formation was promoted by ship emissions in marine environments might have been transported to coastal regions by onshore winds. During spring and especially in summer, higher O_3 concentrations from ships were shifted towards the northeast, while in autumn and winter, high concentrations were shifted to the southeast (Figures 7c, S17 and S18). Due to less irradiation during winter, a seasonal reduction in O_3 concentrations through ship emissions was modeled in the PRD, the YRD and along the Yangtze River. An ozone reduction during winter was also evident in the Bohai and Yellow Seas, where it was plausible that NO_X was transported from northern China and the Korean Peninsula to the marine environment to create VOC-limited conditions. Concentrations were reduced by approximately 10–20 $\mu g \cdot m^{-3}$ (10–20%) in the YRD, PRD and near the Yangtze and by 2 $\mu g \cdot m^{-3}$ (2%) at the northern coastline.

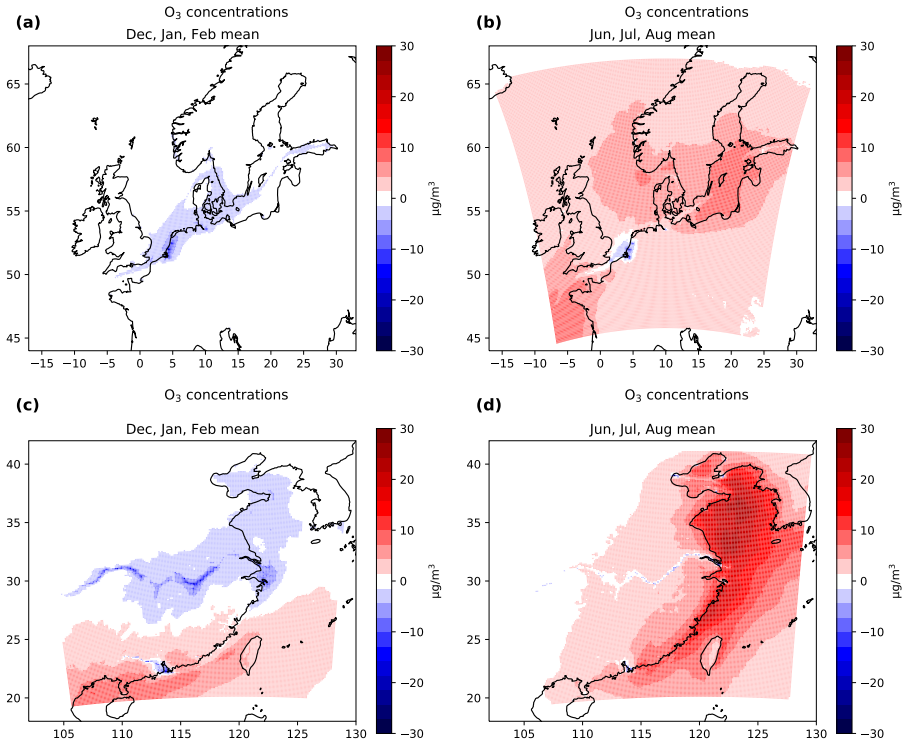

Figure 7. Seasonal averages of O_3 concentrations [$\mu g \cdot m^{-3}$] from shipping in the SC12NSBS domain in Europe for winter (**a**), summer (**b**) and in the CNC12 domain in China for winter (**c**) and summer (**d**).

In contrast to Europe, ozone concentrations in China were less reduced by ship emissions, especially in the large port clusters. This could be attributed to the lower contribution of shipping to total NO_2 concentrations in China. In addition, ship emissions increased ozone formation in many coastal regions that were close to the major shipping lanes. However, in China this observation was much more pronounced than in Europe, as significant amounts of ozone formed in marine areas were transported to land. A similar seasonality for O_3 was modeled for northern Europe and northern China, with lower O_3 concentrations in winter and autumn (Figures 7, S14 and S17). A reversal of this seasonality was found for the subtropical climate zone of southern China.

4.4. Fine Particulate Matter ($PM_{2.5}$)

With respect to its source, $PM_{2.5}$ is divided into primary and secondary particles. Primary $PM_{2.5}$ is emitted directly from the emission source. With respect to ship emis-

sions, these are sulfate, water associated with sulfate, BC, MA and POAs. However, the major impact of $PM_{2.5}$ from shipping usually stems from secondary nitrate and sulfate particles, which are formed in atmospheric chemical reactions from the precursors NO_X and SO_2. Normally, these form as the ammonium salts (Section 4.4.1): ammonium sulfate (Section 4.4.2) and ammonium nitrate (Section 4.4.3). The oxidation rate for these compounds, as well as nucleation and particle growth, depends on environmental parameters (e.g., temperature, solar radiation and humidity). Furthermore, the availability of reaction partners such as ammonia (NH_3), hydroxyl radicals ($OH^{\cdot}$) and ozone (O_3) is of importance. The high atmospheric lifetime of aerosol species enables $PM_{2.5}$ from shipping to be transported hundreds of kilometers away from the main shipping routes to inland areas [89].

In Europe, the highest annual average $PM_{2.5}$ concentrations of 12–15 $\mu g \cdot m^{-3}$ were modeled in neighboring states of the North Sea, close to the major shipping lanes, i.e., northern France, England, northern Germany and especially Belgium and The Netherlands (Figure 8a). In these regions, the formation of secondary aerosols was promoted by high ammonia emissions from agriculture, which were highest during spring, the main season for fertilization (Figure S19); see also Sections 4.4.1–4.4.3).

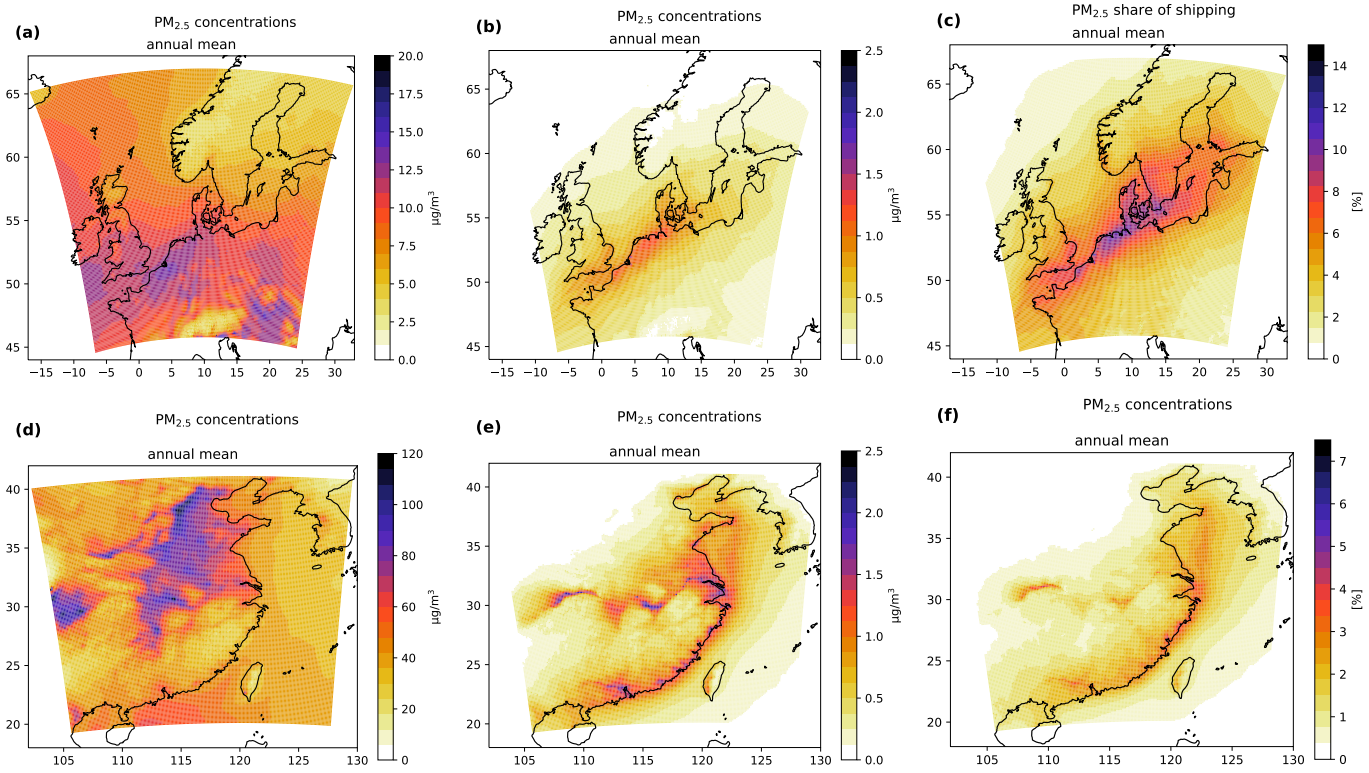

Figure 8. Annual averages of $PM_{2.5}$ concentrations in the SC12NSBS domain in Europe (**a**–**c**) and in the CNC12 domain in China (**d**–**f**). $PM_{2.5}$ concentrations [$\mu g \cdot m^{-3}$] from all emission sources are shown in (**a**,**d**); $PM_{2.5}$ concentrations only from shipping are shown in (**b**,**e**); the share of $PM_{2.5}$ concentrations from shipping in the $PM_{2.5}$ concentrations from all sources [%] is shown in (**c**,**f**).

Ship emissions were relevant precursors for the formation of secondary particulates and contributed approximately 10% to the modeled concentrations (1 to 1.25 $\mu g \cdot m^{-3}$, Figure 8b,c). The main spatial patterns were preserved during all seasons; however, the most impacted region shifted eastwards during winter to northern Germany and Denmark. In summer, the field with the highest concentrations was stretched along the English Channel and the North Sea coastline of the European mainland. This observed shift corresponded to the frequent southwesterly wind direction in winter and the westerly wind directions in summer. During spring, it is evident that ship emissions, combined with the

higher ammonia emissions, result in a strong increase in ship-related $PM_{2.5}$ concentrations (Figure 9c).

In China, the highest annual average concentrations of 100–125 $\mu g \cdot m^{-3}$ were modeled in megacities and regions with high traffic and industry densities, e.g., Chongqing and Chengdu in the Sichuan Basin, Wuhan and the Beijing-Tianjin-Hebei city cluster (Figure 8c). During winter, $PM_{2.5}$ concentrations were highest, with concentrations up to 150–200 $\mu g \cdot m^{-3}$ (Figure S22). Although China has a large agricultural sector, a concise increase in $PM_{2.5}$, promoted by high ammonia emissions from agricultural fertilization, which has its main season here during summer, could not be observed.

$PM_{2.5}$ concentrations of 1–1.5 $\mu g \cdot m^{-3}$ from shipping were modeled along large parts of the Chinese coastline and in the LYP and NCP; concentrations of 2 $\mu g \cdot m^{-3}$ were found in the vicinity of the port cluster in the YRD and PRD and in parts of the Yangtze River. The share of shipping on total $PM_{2.5}$ concentrations in China was 2–3% small due to the high $PM_{2.5}$ contributions from other sectors (Figure 8e,f). Remarkably, almost no ship-related impact on $PM_{2.5}$ concentrations was modeled in northeastern China during winter (Figure 9e). It is assumed that in winter, the ratio of aerosol precursors from other sectors was too high to allow significant particle generation from ship emissions. Furthermore, lower concentrations were modeled for spring and summer along the southern coastline due to the higher temperatures and a higher deposition during the rainy season (Figure 9f,g).

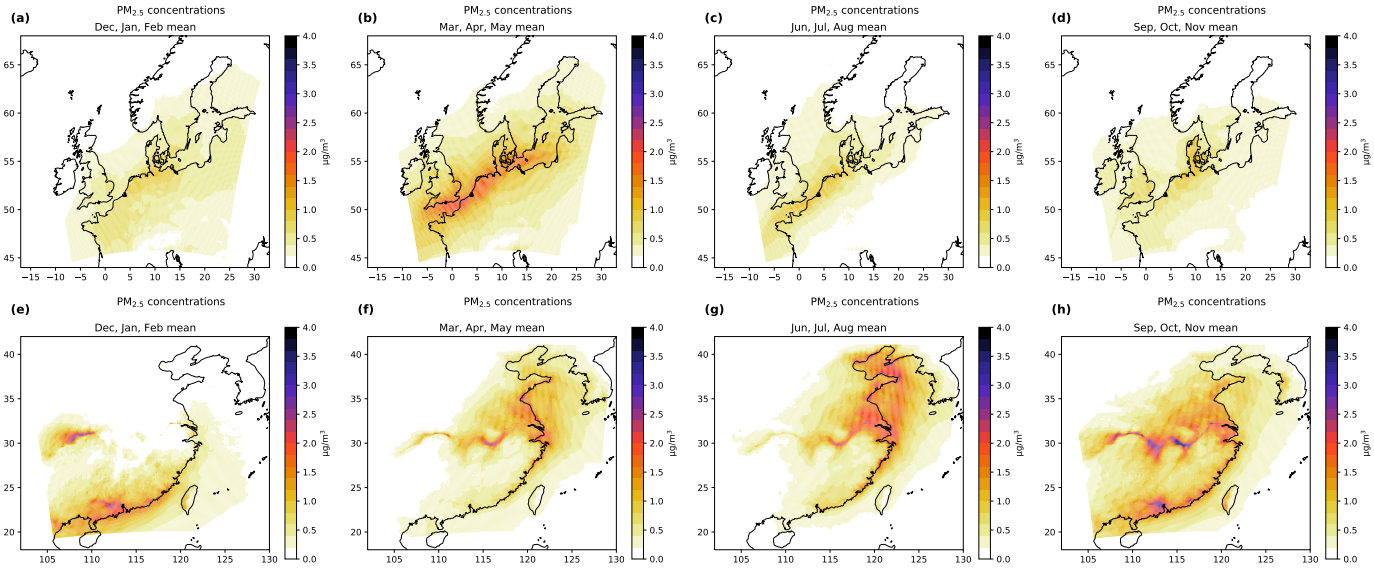

Figure 9. Seasonal averages of $PM_{2.5}$ concentrations [$\mu g \cdot m^{-3}$] from shipping in the SC12NSS domain in Europe for winter (**a**), spring (**b**), summer (**c**), autumn (**d**) and in the CNC12 domain in China for winter (**e**), spring (**f**), summer (**g**) and winter (**h**).

In summary, it can be said that the modeled $PM_{2.5}$ concentrations were approximately 6 times higher in China than in Europe. The $PM_{2.5}$ concentrations due to ship traffic were on a similar level, resulting in a lower contribution from ships to total $PM_{2.5}$ concentrations. Notable differences in seasonality were found between the two regions (Figure 9).

To gain better insight into these aspects, the main components of $PM_{2.5}$, ammonium, sulfate and nitrate concentrations were analyzed for both regions in the following sections. Hereby it was to consider that particle formation is strongly dependent on microclimatic conditions, such as temperature, humidity, concentrations of oxidants and precursors, and the presence of pre-existing aerosols [90,91].

4.4.1. Ammonium (NH_4)

Ammonium is a typical secondary aerosol component originating mainly from agricultural ammonia emissions. The modeled ammonium concentrations presented in this

chapter refer to the NH_4^+ mass component in secondary aerosols, i.e., approximately the sum of the mass of ammonium sulfate and ammonium nitrate particles minus the mass of sulfate and nitrate.

In both regions, a strong seasonality and temperature dependency could be seen for the formation of ammonium particles with higher concentrations during winter and lower concentrations during summer. Seasonality was less pronounced for ammonium from shipping.

In Europe, ammonium originating from ship emissions increased aerosol pollution by 0.2 $\mu g \cdot m^{-3}$ in most coastal regions bordering the main shipping routes (Figure 10b). Analogous to the total $PM_{2.5}$, elevated ammonium concentrations of 0.4 $\mu g \cdot m^{-3}$ were modeled in coastal regions of mainland northern Europe in spring. These are generated by ammonia from agricultural fertilization in combination with ship emissions (Figures S25 and S31). The lowest impact of ammonium from shipping was observed in summer, when high temperatures impeded the nucleation of particles. An approximate contribution of 20% to total ammonium concentrations in Europe could be ascribed to ships (Figure 10c). This contribution could rise up to 40–50% during summer, when fewer precursor species from other emission sectors were present.

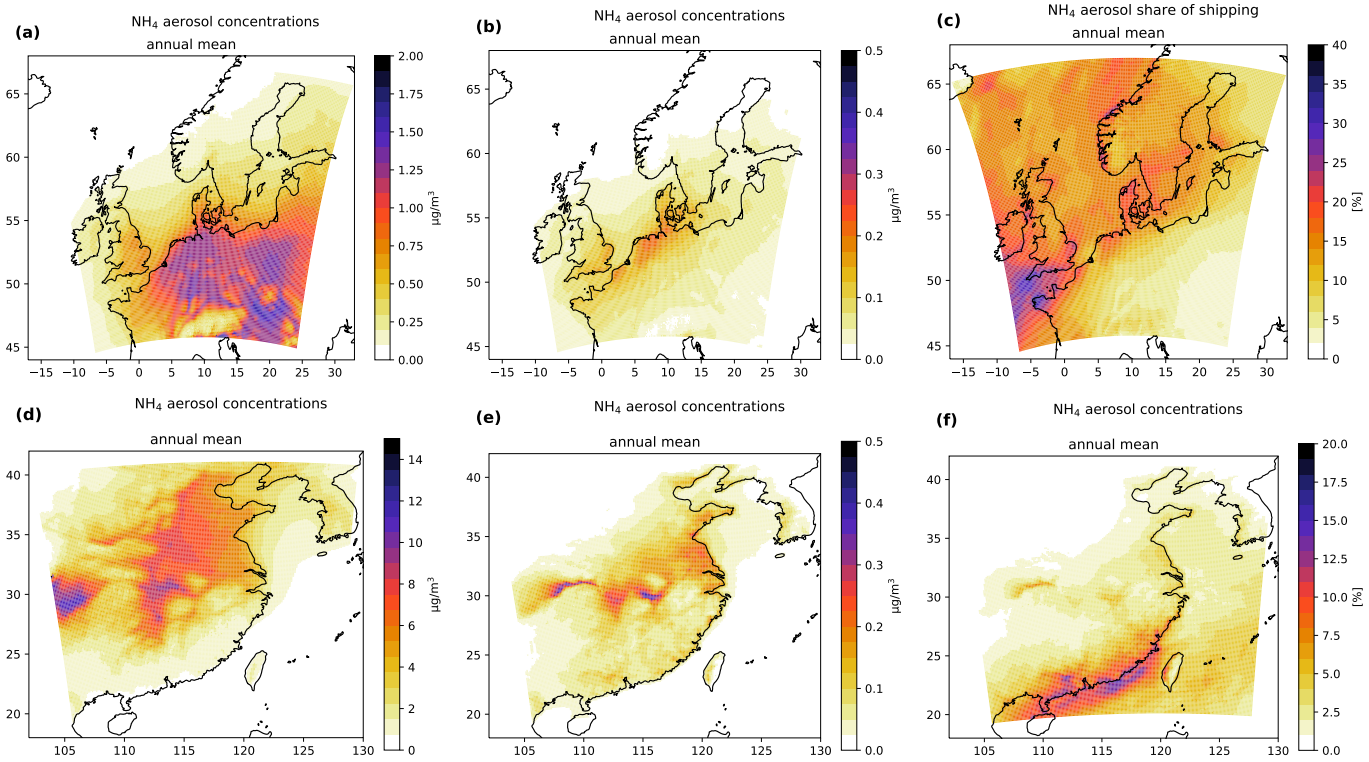

Figure 10. Annual averages of NH_4 concentrations in the SC12NSBS domain in Europe (**a**–**c**) and in the CNC12 domain in China (**d**–**f**). NH_4 concentrations [$\mu g \cdot m^{-3}$] from all emission sources are shown in (**a**,**d**); NH_4 concentrations only from shipping are shown in (**b**,**e**); the share of NH_4 concentrations from shipping in the NH_4 concentrations from all sources [%] is shown in (**c**,**f**).

In China, ammonium from shipping was modeled in concentrations of 0.2 $\mu g \cdot m^{-3}$ along the coastline. Higher concentrations of 0.3–0.4 $\mu g \cdot m^{-3}$ were found in the YRD, along the Yangtze, and in the LYP and the NCP (Figure 10e). The contribution of shipping to ammonium was 12% on the southeast coast and 8% in the northeast coastal regions (Figure 10f). Distinct regional and seasonal differences were evident in the model results. Similar to $PM_{2.5}$, no contribution of shipping to ammonium was modeled in northeast China during winter. Due to the rainy season in spring and summer, almost no ammonium contributions from shipping were modeled at the southern coastline (Figure S29).

A comparison of the two regions showed that ammonium concentrations in China were approximately 5 times higher than those in northern Europe, which was in agreement with the results of the modeled $PM_{2.5}$ totals (Figure 10a,d). The contribution from shipping, however, was in both domains on a similar scale. In China, the spatial pattern of NH_4 concentrations corresponded better to ammonia emissions, which was probably related to the overall higher NH_3 emissions (Figure S28 and S32). Despite the large agricultural sector in China and the high ammonia emissions during summer, no peak NH_4 concentrations from fertilization were modeled, as in Europe during spring. A reason for this could be found in the high deposition rates during the rainy season in summer. Similar to $PM_{2.5}$ concentrations, the remarkable seasonal concentration differences for ammonium from shipping in China were very different from the more uniform seasonality observed in Europe. They could be attributed to the high atmospheric background pollution in China and different weather phenomena.

4.4.2. Sulfate (SO_4)

Sulfate particles form from SO_2 in the atmosphere via a photoinduced gas-phase oxidation over the intermediate SO_3 or in an aqueous phase reaction. Sulfate is deposited as sulfuric acid or irreversibly combines with ammonium in a reaction favored over the formation of ammonium nitrate [92].

In both domains, sulfate concentrations corresponded to the spatial and seasonal patterns of SO_2 concentrations, although they were more diffuse due to a longer particle lifetime. Accordingly, sulfate from shipping played a subordinate role in the area of the northern European SECA (see also Section 4.2). However, SO_2 emitted in the Celtic Sea, outside the SECA, was able to form aerosols that were transported by westerly winds to the United Kingdom and the French coastline in concentrations of approximately 0.1 to 0.15 $\mu g \cdot m^{-3}$ (Figure 11b). Sulfate concentrations were highest during summer due to increased shipping activity (Figure S43).

In China, sulfate from shipping impacts the air quality along the whole coastline and along the Yangtze River. The highest concentrations of approximately 0.5 $\mu g \cdot m^{-3}$ (5–10%) were found near the port cluster in the YRD and PRD (Figure 11e). Similar to $PM_{2.5}$ and ammonium, almost no SO_4 concentrations from shipping were modeled in northeastern China during winter, while in summer, concentrations were reduced in southeastern China due to the rainy season (Figure S43). When compared to other particulates, SO_4 from shipping was found closer to shipping lanes and coastal regions, which could be explained by its higher affinity to ammonium compared to nitrate.

4.4.3. Nitrate (NO_3)

Nitrate particles form from NO_2 in a gas-phase oxidation with hydroxyl radicals during the day or via the intermediate N_2O_5 in a nightly oxidation by ozone. Nitrate is deposited from the atmosphere as nitric acid or reacts with ammonia to form ammonium nitrate particles.

In Europe, especially the coastal regions bordering the English Channel, northern France, Belgium, The Netherlands, northern Germany and Denmark were affected by high NO_3 loads (Figure 12b). In winter and autumn, higher concentrations were shifted towards the northeastern coastline of the European mainland, while in summer, they were shifted towards the southwest. Due to agricultural fertilization, NO_3 concentrations were 1.5 $\mu g \cdot m^{-3}$ highest during spring (Figure S34).

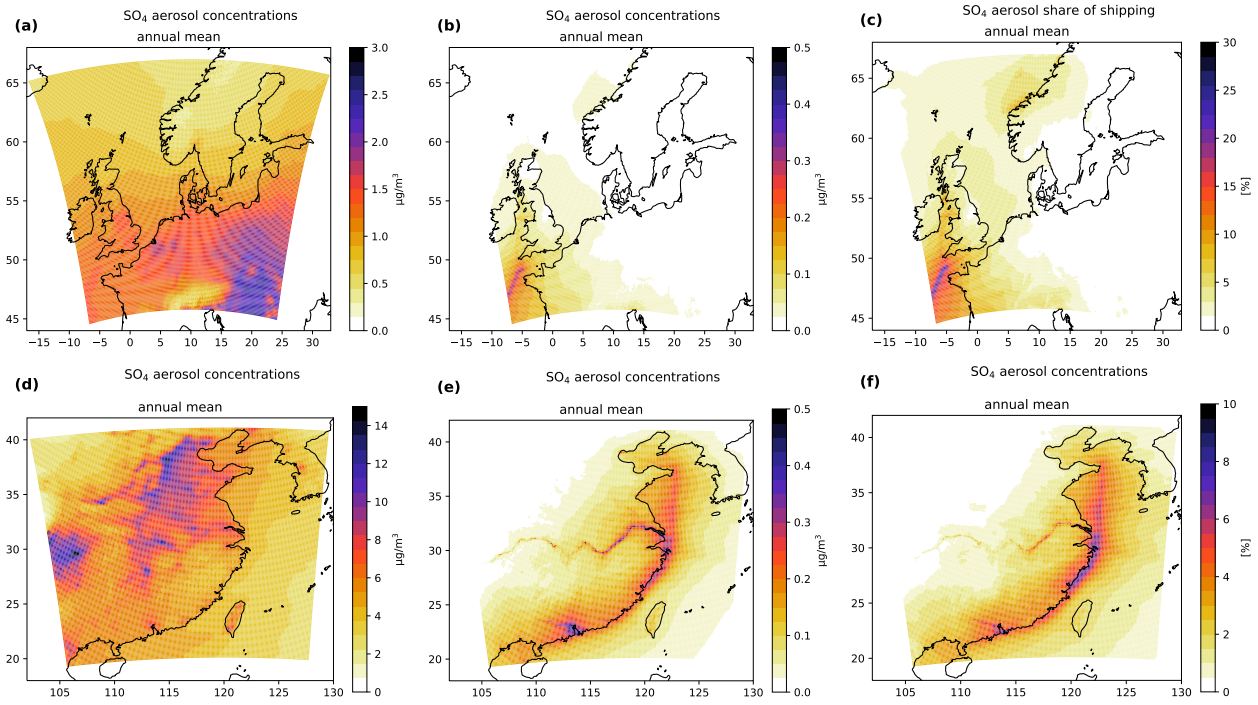

Figure 11. Annual averages of SO_4 concentrations in the SC12NSBS domain in Europe (**a**–**c**) and in the CNC12 domain in China (**d**–**f**). SO_4 concentrations [$\mu g \cdot m^{-3}$] from all emission sources are shown in (**a**,**d**); SO_4 concentrations only from shipping are shown in (**b**,**e**); the share of SO_4 concentrations from shipping in the SO_4 concentrations from all sources [%] is shown in (**c**) and (**f**).

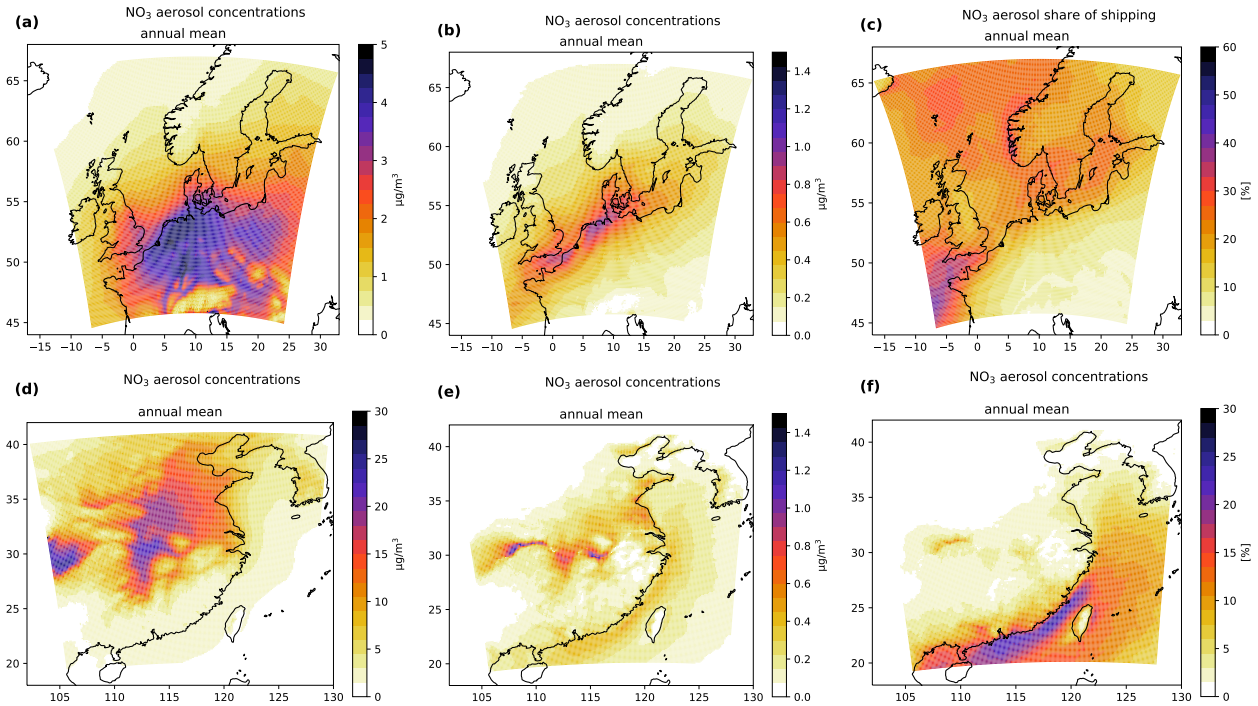

Figure 12. Annual averages of NO_3 concentrations in the SC12NSBS domain in Europe (**a**–**c**) and in the CNC12 domain in China (**d**–**f**). NO_3 concentrations [$\mu g \cdot m^{-3}$] from all emission sources are shown in (**a**,**d**); NO_3 concentrations only from shipping are shown in (**b**,**e**); the share of NO_3 concentrations from shipping in the NO_3 concentrations from all sources [%] is shown in (**c**,**f**).

In China, the Yangtze River, the LYP and NCP were most affected by nitrate aerosols from shipping in concentrations of 0.5–1 $\mu g \cdot m^{-3}$ (Figure 12e). The highest concentrations of 1 $\mu g \cdot m^{-3}$ were modeled during spring (Figure S37).

In both regions nitrate concentrations were found to correlate with ammonium concentrations. Especially in China, high NO_3 concentrations were modeled in areas with low SO_2 concentrations but abundant ammonium (Figure 12a,d). In general, the formation rate of NO_3 particles showed a stronger seasonality than sulfate. A comparison of the nitrate and NO_2 ratios suggested that the formation of nitrate aerosols was limited by available ammonium. The NO_3 and NH_4 concentrations were approximately 5 times higher in China than in Europe, while the ratio for NO_2 was only 2.5. The highest NO_3 concentrations were modeled in winter, when low temperatures enabled higher nucleation rates. Due to the SECA in the North and Baltic Seas, SO_2 concentrations were smaller than those China, and emissions from regional shipping resulted in higher NO_3 concentrations (Figure 12b).

5. Conclusions

In this work, an air quality modelling system was applied to calculate and study pollutant concentrations for northern Europe, including the North and Baltic Seas, and eastern China, including the Yellow and South China Seas for 2015 in a harmonized approach. However, a noticeable difference between these two regions was, generally, the background air pollution, which could be classified as high in China and medium in Northern Europe. The goal of this study was a comparison of the impact of ship emissions between both regions, with a focus on the obvious differences and similarities.

An accurate representation of ship emissions was achieved by using two temporally and spatially high resolved bottom-up ship emission inventories, both created with the MoSES ship emission model using comparable input parameters. Anthropogenic emissions from other sectors were covered by the MEIC and EDGAR emissions inventories for China and CAMS emissions for Europe, which were distributed and generated using the HiMEMO emissions model. The emission data were fed into the chemical transport model CMAQ, as well as the meteorologic forcing, which was calculated with COSMO-CLM. Species concentrations of interest were those for NO_2, SO_2, O_3, PM and the secondary aerosol components ammonia, sulfate and nitrate. The contribution of ship traffic to air pollutant concentrations was determined by using the zero-out method.

The performance of the model was evaluated by a comparison of the modeled concentrations with measurement data from coastal air quality stations. Overall, the model performance proved to be satisfactory. However, NO_2 concentrations were often predicted to be to low for Europe, and ozone concentrations were often predicted to be too high in both regions. A comparison between the results obtained with the MEIC inventory and the results obtained with the EDGAR v5 inventory for nonshipping land-based anthropogenic emissions in China pointed to an overestimation by the latter.

The comparison between China and Europe showed that air pollutant concentrations originating from ship emission were generally on a comparable scale, with slightly higher concentrations in China. However, a stronger seasonality was found for China, with the East Asian monsoon and different climate zones as an important factors. Greater similarity was found between temperate northeastern China and Europe, while in the subtropical climate zone, the observed trends were often reversed. Compared to Europe, the overall higher concentrations of background air pollution in China modified the atmospheric chemistry of ship exhausts, especially for PM. This resulted in a smaller relative impact of ship emissions in China.

The relative contribution of ships to NO_2 concentrations was higher in Europe, with 30% in moderately affected regions and 50% in highly affected regions, compared to 10% and 30% in China. In addition, NO_2 was transported further in the atmosphere during winter in China, which was related to an increased NO_2 lifetime due to oxidant-limited conditions.

As a result of the SECA implemented in the North and Baltic Seas in 2015, the amount of SO_2 emissions differed significantly between the compared regions.

Tropospheric ozone reductions through ship emissions in large ports were stronger in Europe than in China, by an average of 10–15 $\mu g \cdot m^{-3}$ (10–15%). In China's large ports, the shipping influence on ozone concentrations was mainly neutral due to the lower contribution of ships to total emissions. Along the Chinese coast, ship emissions had a stronger promoting effect on O_3 formation, particularly in the south, with 2–10 $\mu g \cdot m^{-3}$ (3–10%). In southern China, this could be attributed to a higher irradiation but also, an inland transport of ozone, whose formation is promoted by shipping in marine environments, was plausible.

In Europe, NO_X and SO_2 from shipping led in combination with high ammonia emissions from agricultural fertilization during spring to peaking secondary PM concentrations (2 $\mu g \cdot m^{-3}$, 13%). A similar seasonal peak of secondary PM could not be observed in China, despite high ammonia emissions from its large agricultural sector. Another notable observation was that during winter, no significant $PM_{2.5}$ concentrations from shipping were modeled in the eastern and northeastern parts of China. High aerosol precursor emissions from other sectors could deplete the reaction partners and oxidants necessary for secondary particle formation and inhibit the transformation of aerosol precursors from ship exhausts.

A comparison of the obtained model results with former studies by Aulinger et al. [22] on the North Sea and Karl et al. [23] on the Baltic Sea, both for 2011, showed a similar impact of shipping on NO_2 concentrations. The results for SO_2 were not comparable due to differences in the sulfur regulation between these years. The impacts of ships on ozone concentrations were modeled slightly higher in this study for both, a promotion of ozone formation and depletion. $PM_{2.5}$ concentrations from ships were slightly lower in this study, which was reasonable due to the stricter fuel sulfur limits in 2015. Former studies on the impact of ship emissions on air quality for the YRD and PRD in 2015, by Feng et al. [35] and Chen et al. [93], respectively, were for most pollutants in agreement with the concentrations found in this study. However, the ozone reducing effect of ship emissions in the PRD was also found to be stronger in the present study.

The results from this study show the importance for a regulation of ship emissions in concert with other emission sectors, particularly in China. Otherwise, potential achievements from reducing ship emissions could be offset by emissions from other sectors. Indicators for such effects were the prolonged NO_X lifetime and the impeded formation of secondary PM from ship emissions found in northern China. Furthermore this was indicated by the fact that ship-related $PM_{2.5}$ concentrations were in a similar range between Europe and China although sulfur-containing ship emissions, as precursors to secondary PM, were drastically reduced in Europe due to the implemented SECA. Since ammonia is an important precursor for ship-related PM, a regulation of NH_3 emissions could help in reducing PM concentrations. Such regulations could include a motivation to limit agricultural fertilization to specific seasons or by fertilization recommendations based on the current meteorologic situation to mitigate PM formation.

Supplementary Materials: The following supporting information can be downloaded at: https://www.mdpi.com/article/10.3390/atmos13060894/s1.

Author Contributions: Conceptualization, D.A.S., V.M. and M.Q.; methodology, D.A.S., R.P., V.M. and M.Q.; software, D.A.S. and R.P.; validation, D.A.S.; formal analysis, D.A.S.; investigation, D.A.S., R.P. and G.Y.; resources, V.M. and Y.Z.; data curation, D.A.S. and R.P.; writing—original draft preparation, D.A.S., R.P., G.Y.; writing—review and editing, R.P., V.M., M.Q., G.Y., Y.Z.; visualization, D.A.S.; supervision, V.M., M.Q. and Y.Z.; project administration, V.M., M.Q. and Y.Z.; funding acquisition, V.M. and M.Q. All authors have read and agreed to the published version of the manuscript.

Funding: This research and APC were funded by the German Research Foundation (DFG) in the framework of the DFG-NSFC funded project "ShipChem" with the DFG project nr. 645514 and supported by the BSH funded project "SeAir" (BSH contract code: 10042629, Hereon contract code: 430/2018).

Institutional Review Board Statement: Not applicable.

Informed Consent Statement: Not applicable.

Data Availability Statement: The data presented in this study are available on request from the corresponding author.

Conflicts of Interest: The authors declare no conflict of interest. The funders had no role in the design of the study; in the collection, analyses, or interpretation of data; in the writing of the manuscript, or in the decision to publish the results.

Abbreviations

The following abbreviations are used in this manuscript:

AIS	Automatic Identification System
AQER	Air Quality e-Reporting
BC	Black Carbon
BSH	German Federal Office for Sea Shipping and Hydrography
CAMS	Copernicus Atmosphere Monitoring Service
CMAQ	Community Multi-scale Air Quality model
CNC12	Descriptor for the domain located in China
CNSS	Clean North Sea Shipping
COSMOS-CLM	Consortium for Small Scale Modelling in Climate Mode
DECA	Domestic Emission Control Area
ECA	Emission Control Area
ECCAD	Emissions of atmospheric Compounds and Compilation of Ancillary Data
ECMWF	European Centre for Medium-Range Weather Forecasts
EDGAR	Emissions Database for Global Atmospheric Research
EF	Emission Factor
EI	Emission Inventory
EMSA	European Maritime Safety Agency
FMI	Finnish Meteorological Institute
GNFR	Guidelines for reporting emissions and projections data Nomenclature For Reporting
HiMEMO	Highly Modular Emission Model
IMO	International Maritime Organization
IFS	Integrated Forecast System
IPCC	Intergovernmental Panel on Climate Change
LAI	Leaf Area Index
LYP	Lower Yangtze Plain
MA	Mineral Ash
MARPOL	International Convention for Prevention of Marine Pollution For Ships
MARS	Meteorological Archival and Retrieval System
MEGAN	Model of Emissions of Gases and Aerosols from Nature
MEIC	Multiresolution Emission Inventory for China
MoSES	Modular Ship Emission modeling System
NCP	North China Plain
NECA	Nitrogen Emission Control Area
NMB	Normalized Mean Bias
NMVOC	Nonmethane Organic Volatile Compounds
OC	Organic Compounds
PM	Particulate Matter
POA	Primary Organic Aerosol
PRD	Pearl River Delta
RCEP	Regional Comprehensive Economic Partnership
SC12NSBS	Descriptor for the domain located in northern Europe
SECA	Sulfur Emission Control Area
SHEBA	Sustainable Shipping and the Environment of the Baltic Sea Region
SNAP	Selected Nomenclature for Air Pollution
STEAM	Ship Traffic Emissions Assessment Model
TEU	Twenty-foot Equivalent Unit
TNO	The Netherlands Organisation for Applied Scientific Research
VOC	Volatile Organic Compounds
YRD	Yangtze River Delta

Appendix A. Model Performance Data

In the following Tables A1 and A2, the comparison data of the modeled "base" case with the measurements is shown for all considered stations. For the more elaborate tables that include the geometric mean, the normalized mean bias (NMB) and the Spearman correlation coefficient calculated for all stations, for each pollutant for the "base" and the"no ships" case, as well as the number of the available hourly measurements the reader is referred to Section S2 of the supplementary material.

Table A1. Comparison of modeled NO_2, SO_2, O_3 8-h mean and fine particulate matter ($PM_{2.5}$) concentrations of the modeled "base" case in $\mu g \cdot m^{-3}$ with measurements in the SC12NSBS domain. Additionally, the mean correlation coefficient (Mean Corr.) and two values, calculated as the mean of either positive or negative NMBs are shown (NMB_{pos}, NMB_{neg}). For the latter two values, the number of stations used for the calculation is given in parentheses.

	NO_2		SO_2		O_3 8-h Mean		$PM_{2.5}$	
Station	**$Mean_{model}$**	**$Mean_{meas}$**	**$Mean_{model}$**	**$Mean_{meas}$**	**$Mean_{model}$**	**$Mean_{meas}$**	**$Mean_{model}$**	**$Mean_{meas}$**
Oismäe	3.65	5.13	0.39	0.47	67.60	51.05	—	—
Phare d'Ailly	—	—	—	—	76.09	59.62	—	—
Schoten	17.79	21.26	—	—	45.04	29.50	10.87	10.79
Utö	1.16	2.25	0.10	0.30	74.56	66.32	4.00	3.45
Newcastle	6.06	25.56	—	—	66.52	36.56	7.96	7.80
Århus	3.23	9.61	—	—	72.37	50.36	—	—
Westerland	1.34	2.17	0.09	0.26	77.55	61.91	—	—
De Zilk	12.99	9.83	0.73	0.95	48.49	42.27	9.73	6.61
Den Haag	17.91	22.20	—	—	39.51	33.29	—	—
Wieringerwerf	5.30	8.55	—	—	68.96	44.15	8.93	6.04
Pyykösjärvi	3.00	6.61	—	—	51.92	43.39	—	—
Råö	—	—	—	—	74.34	62.74	—	—
Brighton	4.77	10.72	—	—	72.40	51.52	—	—
Plymouth	2.27	13.53	—	—	76.77	45.59	8.52	9.33
Narberth	1.60	1.63	0.37	0.68	75.12	61.09	—	—
Blackpool	2.47	11.46	—	—	68.55	49.39	8.17	5.78
Dublin	3.05	4.94	—	—	—	—	—	—
Hamburg	12.12	26.39	1.07	3.28	—	—	—	—
Lahemaa	1.33	1.61	0.23	0.53	65.52	50.24	—	—
Ostfries. Inseln	3.43	6.39	0.14	0.40	72.08	55.72	—	—
Elbmündung	5.33	9.56	—	—	67.33	47.54	—	—
Virolahti	1.56	2.74	0.26	0.21	67.24	47.51	3.87	4.19
Vilsandi	0.98	1.37	0.11	0.27	75.61	65.64	—	—
Copenhagen	7.13	12.32	—	—	66.14	53.76	—	—
Ulborg	1.54	2.77	—	—	73.55	61.99	—	—
Kallio	5.90	14.01	1.00	0.61	58.39	44.94	4.84	4.22
Houtem	7.19	7.12	1.19	1.07	64.51	47.15	9.65	8.12
Gent	13.51	23.40	0.94	1.23	50.48	32.78	10.57	11.15
Lullington Heath	4.44	4.79	0.28	0.95	73.98	53.61	—	—
Zingst	2.95	3.73	0.21	0.39	72.69	57.10	—	—
Gdańsk Nowy Port	5.80	10.44	1.67	2.17	—	—	—	—
Mean NMB_{pos}	0.398 (1)		0.365 (10)		0.27 (28)		0.164 (9)	
Mean NMB_{neg}	−0.38 (28)		−0.266 (6)		n.a. (0)		−0.03 (2)	
Mean Corr.	0.617		0.279		0.659		0.377	

Table A2. Comparison of modeled NO_2, SO_2, O_3 8-h mean and $PM_{2.5}$ concentrations of the modeled "base" case in $\mu g \cdot m^{-3}$ with measurements in the CNC12 domain. Additionally, the mean correlation coefficient (Mean Corr.) and two values, calculated as the mean of either positive or negative NMBs are shown (NMB_{pos}, NMB_{neg}). For the latter two values, the number of stations used for the calculation is given in parentheses.

	NO_2		SO_2		O_3 8-h Mean		$PM_{2.5}$	
Station	**$Mean_{model}$**	**$Mean_{meas}$**	**$Mean_{model}$**	**$Mean_{meas}$**	**$Mean_{model}$**	**$Mean_{meas}$**	**$Mean_{model}$**	**$Mean_{meas}$**
Dalian	53.68	29.53	24.74	19.59	26.28	64.12	43.42	33.98
Huludao	16.78	29.73	7.85	33.10	52.85	48.38	31.79	40.38
Qinhuangdao	29.04	38.01	14.51	28.64	31.46	30.50	38.45	30.11
Tianjin	56.95	33.53	29.83	19.00	4.32	29.99	59.93	50.52
Lianyungang	15.05	24.31	4.75	22.07	57.19	60.35	42.26	39.82
Yancheng	18.57	19.60	3.75	15.53	59.14	72.76	41.12	35.52
Nantong	36.79	30.45	11.84	23.50	37.06	62.88	42.19	45.28
Shanghai	59.11	39.21	27.09	14.70	21.57	60.07	41.51	41.10
Ningbo	44.97	37.27	16.06	14.36	36.73	50.95	37.51	35.30
Wenzhou	30.72	38.75	9.05	11.96	51.90	33.98	36.03	37.29
Fuzhou	23.77	28.92	6.19	5.78	70.80	40.27	34.67	24.41
Quanzhou	24.96	21.22	9.87	8.60	63.49	46.82	44.64	23.66
Shantou	15.01	16.98	6.05	11.64	78.48	61.95	42.11	28.22
Shenzhen	47.27	30.07	15.55	7.93	27.79	48.69	48.70	25.08
Guangzhou	58.01	41.38	20.86	10.96	22.08	26.21	52.25	32.91
Zhongshan	20.33	23.39	7.03	9.99	64.65	33.83	48.02	26.30
Zhuhai	14.25	23.30	5.03	7.03	79.18	51.72	45.85	23.98
Haikou	6.92	11.34	2.98	4.84	85.70	44.20	37.56	17.73
Beihai	5.38	12.10	4.93	7.90	92.03	65.84	42.38	19.20
Fangchenggang	5.04	10.45	4.48	4.89	87.99	36.73	41.99	24.14
Mean, NMB_{pos}	0.402 (12)		0.512 (9)		0.544 (18)		0.439 (17)	
Mean, NMB_{neg}	−0.283 (8)		−0.38 (11)		−0.1 (2)		−0.06 (3)	
Mean Corr.	0.477		0.398		0.628		0.408	

References

1. UNCTAD. *Review of Maritime Transport 2020*; Technical Report; United Nations Conference on Trade and Development: Geneva, Switzerland, 2020.
2. IMO. *Second IMO Greenhouse Gas Study 2009*; Technical Report; International Maritime Organisation: London, UK, 2009.
3. IMO. *Third IMO Greenhouse Gas Study 2014*; Technical Report: IMO: London, UK, 2014. https://doi.org/10.1007/s10584-013-0912-3.
4. Corbett, J.J.; Winebrake, J.J.; Green, E.H.; Kasibhatla, P.; Eyring, V.; Lauer, A. Mortality from ship emissions: A global assessment. *Environ. Sci. Technol.* **2007**, *41*, 8512–8518. https://doi.org/10.1021/es071686z.
5. Dalsøren, S.B.; Eide, M.S.; Endresen, O.; Mjelde, A.; Gravir, G.; Isaksen, I.S. Update on emissions and environmental impacts from the international fleet of ships: The contribution from major ship types and ports. *Atmos. Chem. Phys.* **2009**, *9*, 2171–2194. https://doi.org/10.5194/acp-9-2171-2009.
6. Liu, H.; Fu, M.; Jin, X.; Shang, Y.; Shindell, D.; Faluvegi, G.; Shindell, C.; He, K. Health and climate impacts of ocean-going vessels in East Asia. *Nat. Clim. Chang.* **2016**, *6*, 1037–1041. https://doi.org/10.1038/nclimate3083.
7. Sofiev, M.; Winebrake, J.J.; Johansson, L.; Carr, E.W.; Prank, M.; Soares, J.; Vira, J.; Kouznetsov, R.; Jalkanen, J.P.; Corbett, J.J. Cleaner fuels for ships provide public health benefits with climate tradeoffs. *Nat. Commun.* **2018**, *9*, 1–12. https://doi.org/10.1038/s41467-017-02774-9.
8. Hassellöv, I.M.; Turner, D.R.; Lauer, A.; Corbett, J.J. Shipping contributes to ocean acidification. *Geophys. Res. Lett.* **2013**, *40*, 2731–2736. https://doi.org/10.1002/grl.50521.
9. Eyring, V.; Isaksen, I.S.; Berntsen, T.; Collins, W.J.; Corbett, J.J.; Endresen, O.; Grainger, R.G.; Moldanova, J.; Schlager, H.; Stevenson, D.S. Transport impacts on atmosphere and climate: Shipping. *Atmos. Environ.* **2010**, *44*, 4735–4771. https://doi.org/10.1016/j.atmosenv.2009.04.059.
10. Lu, X.; Zhang, L.; Shen, L. Meteorology and Climate Influences on Tropospheric Ozone: A Review of Natural Sources, Chemistry, and Transport Patterns. *Curr. Pollut. Rep.* **2019**, *5*, 238–260. https://doi.org/10.1007/s40726-019-00118-3.
11. IMO MEPC. *Resolution MEPC.75(40) Protocol to the MARPOL Convention with added Annex VI,*; Technical Report; IMO: London, UK, 1997.
12. IMO MEPC. *MEPC*; Technical Report; IMO: London, UK, 2008; Volume 176.
13. IMO MEPC. *MEPC 70/INF.34*; Technical Report; IMO: London, UK, 2016.
14. Corbett, J.J.; Fischbeck, P. Emissions from ships. *Science* **1997**, *278*, 823–824. https://doi.org/10.1126/science.278.5339.823.

15. Endresen, Ø.; Sørgård, E.; Sundet, J.K.; Dalsøren, S.B.; Isaksen, I.S.A.; Berglen, T.F.; Gravir, G. Emission from international sea transportation and environmental impact. *J. Geophys. Res.* **2003**, *108*, 4560. https://doi.org/10.1029/2002JD002898.
16. Eyring, V.; Köhler, H.W.; Aardenne, J.V.; Lauer, A. Emissions from international shipping: 1. The last 50 years. *J. Geophys. Res. D Atmos.* **2005**, *110*, 171–182. https://doi.org/10.1029/2004JD005619.
17. Eyring, V.; Köhler, H.W.; Lauer, A.; Lemper, B. Emissions from international shipping: 2. Impact of future technologies on scenarios until 2050. *J. Geophys. Res. D Atmos.* **2005**, *110*, 183–200. https://doi.org/10.1029/2004JD005620.
18. Dentener, F.; Kinne, S.; Bond, T.; Boucher, O.; Cofala, J.; Generoso, S.; Ginoux, P.; Gong, S.; Hoelzemann, J.J.; Ito, A.; et al. Emissions of primary aerosol and precursor gases in the years 2000 and 1750 prescribed data-sets for AeroCom. *Atmos. Chem. Phys.* **2006**, *6*, 4321–4344. https://doi.org/10.5194/acp-6-4321-2006.
19. Lauer, A.; Eyring, V.; Corbett, J.J.; Wang, C.; Winebrake, J.J. Assessment of near-future policy instruments for oceangoing shipping: Impact on atmospheric aerosol burdens and the earth's radiation budget. *Environ. Sci. Technol.* **2009**, *43*, 5592–5598. https://doi.org/10.1021/es900922h.
20. Matthias, V.; Bewersdorff, I.; Aulinger, A.; Quante, M. The contribution of ship emissions to air pollution in the North Sea regions. *Environ. Pollut.* **2010**, *158*, 2241–2250. https://doi.org/10.1016/j.envpol.2010.02.013.
21. Jonson, J.E.; Jalkanen, J.P.; Johansson, L.; Gauss, M.; Gon, H.A.V.D. Model calculations of the effects of present and future emissions of air pollutants from shipping in the Baltic Sea and the North Sea. *Atmos. Chem. Phys.* **2015**, *15*, 783–798. https://doi.org/10.5194/acp-15-783-2015.
22. Aulinger, A.; Matthias, V.; Zeretzke, M.; Bieser, J.; Quante, M.; Backes, A. The impact of shipping emissions on air pollution in the Greater North Sea region—Part 1: Current emissions and concentrations. *Atmos. Chem. Phys. Discuss.* **2016**, *15*, 11277–11323. https://doi.org/10.5194/acpd-15-11277-2015.
23. Karl, M.; Jonson, J.E.; Uppstu, A.; Aulinger, A.; Prank, M.; Sofiev, M.; Jalkanen, J.P.; Johansson, L.; Quante, M.; Matthias, V. Effects of ship emissions on air quality in the Baltic Sea region simulated with three different chemistry transport models. *Atmos. Chem. Phys.* **2019**, *19*, 7019–7053. https://doi.org/10.5194/acp-19-7019-2019.
24. Jonson, J.E.; Gauss, M.; Schulz, M.; Jalkanen, J.P.; Fagerli, H. Effects of global ship emissions on European air pollution levels. *Atmos. Chem. Phys.* **2020**, *20*, 11399–11422. https://doi.org/10.5194/acp-20-11399-2020.
25. CNSS Project. *Clean North Sea Shipping Final Report: Key Findings and Recommendations*; Technical Report; CNSS: Bergen, Norway, 2014. Available online: https://www.hereon.de/imperia/md/images/hzg/presse/pressemitteilungen/imperiamdimagesgkssppressepressemitteilungen2014/cnss_finalreport.pdf accessed on 30 May 2022.
26. SHEBA Project. Sustainable Shipping and Environment of the Baltic Sea Region. 2018. Available online: https://www.sheba-project.eu/ (accessed on 26 January 2021).
27. Hoesly, R.M.; Smith, S.J.; Feng, L.; Klimont, Z.; Janssens-Maenhout, G.; Pitkanen, T.; Seibert, J.J.; Vu, L.; Andres, R.J.; Bolt, R.M.; et al. Historical (1750–2014) anthropogenic emissions of reactive gases and aerosols from the Community Emissions Data System (CEDS). *Geosci. Model Dev.* **2018**, *11*, 369–408.
28. Zhang, Q.; He, K.; Hong, H. Cleaning China's air. *Nature* **2012**, *484*, 161–162. https://doi.org/10.1038/484161a.
29. China State Council. Action Plan on Prevention and Control of Air Pollution. 2013. Available online: http://www.gov.cn/zwgk/2013-09/12/content_2486773.htm (accessed on 21 January 2021).
30. China. Air Quality Targets Set by the Action Plan Have Been Fully Realized. 2018. Available online: http://www.gov.cn/xinwen/2018-02/01/content_5262720.htm (accessed on 21 January 2021).
31. Lloyds' List. One Hundred Ports 2020. Available online: https://lloydslist.maritimeintelligence.informa.com/one-hundred-container-ports-2020 (accessed on 22 January 2021).
32. UNCTAD STAT. Maritime Profile: China. Available online: https://unctadstat.unctad.org/countryprofile/maritimeprofile/en-gb/156/index.html (accessed on 22 January 2021).
33. China Ministry of Transport. *Action Plan to Establish a National Emission Control Area for Ship Emission Control*; Technical Report; China Ministry of Transport: Beijing, China, 2018.
34. Liu, H.; Jin, X.; Wu, L.; Wang, X.; Fu, M.; Lv, Z.; Morawska, L.; Huang, F.; He, K. The impact of marine shipping and its DECA control on air quality in the Pearl River Delta, China. *Sci. Total Environ.* **2018**, *625*, 1476–1485. https://doi.org/10.1016/j.scitotenv.2018.01.033.
35. Feng, J.; Zhang, Y.; Li, S.; Mao, J.; Patton, A.; Zhou, Y.; Ma, W.; Liu, C.; Kan, H.; Huang, C.; et al. The influence of spatiality on shipping emissions, air quality and potential human exposure in the Yangtze River Delta/Shanghai, China. *Atmos. Chem. Phys.* **2019**, *19*, 6167–6183. https://doi.org/10.5194/acp-19-6167-2019.
36. Zhao, J.; Zhang, Y.; Patton, A.P.; Ma, W.; Kan, H.; Wu, L.; Fung, F.; Wang, S.; Ding, D.; Walker, K. Projection of ship emissions and their impact on air quality in 2030 in Yangtze River delta, China. *Environ. Pollut.* **2020**, *263*, 114643. https://doi.org/10.1016/j.envpol.2020.114643.
37. Schwarzkopf, D.A.; Petrik, R.; Matthias, V.; Quante, M.; Majamäki, E.; Jalkanen, J.P. A ship emission modeling system with scenario capabilities. *Atmos. Environ. X* **2021**, *12*, 100132. https://doi.org/10.1016/j.aeaoa.2021.100132.
38. Byun, D.W.; Ching, J.K.S. *Science Algorithms of the EPA Models-3 Community Multiscale Air Quality (CMAQ) Modeling System*; Technical Report; United States Environmental Protection Agency: Washington, DC, USA, 1999.
39. Byun, D.; Schere, K.L. Review of the governing equations, computational algorithms, and other components of the models-3 Community Multiscale Air Quality (CMAQ) modeling system. *Appl. Mech. Rev.* **2006**, *59*, 51–76. https://doi.org/10.1115/1.2128636.

40. Yarwood, G.; Rao, S.; Yocke, M.; Whitten, G. Updates to the Carbon Bond Mechanism: CB05; Technical Report; United States Environmental Protection Agency: Washington, DC, USA, 2005.
41. Whitten, G.Z.; Heo, G.; Kimura, Y.; McDonald-Buller, E.; Allen, D.T.; Carter, W.P.; Yarwood, G. A new condensed toluene mechanism for Carbon Bond: CB05-TU. *Atmos. Environ.* **2010**, *44*, 5346–5355. https://doi.org/10.1016/j.atmosenv.2009.12.029.
42. Sarwar, G.; Appel, K.W.; Carlton, A.G.; Mathur, R.; Schere, K.; Zhang, R.; Majeed, M.A. Impact of a new condensed toluene mechanism on air quality model predictions in the US. *Geosci. Model Dev.* **2011**, *4*, 183–193. https://doi.org/10.5194/gmd-4-183-2011.
43. Inness, A.; Ades, M.; Agustí-Panareda, A.; Barr, J.; Benedictow, A.; Blechschmidt, A.M.; Dominguez, J.J.; Engelen, R.; Eskes, H.; Flemming, J.; et al. The CAMS reanalysis of atmospheric composition. *Atmos. Chem. Phys.* **2019**, *19*, 3515–3556. https://doi.org/10.5194/acp-19-3515-2019.
44. ECMWF-CAMS. Data Store. 2021. Available online: https://ads.atmosphere.copernicus.eu/cdsapp#!/dataset/cams-global-reanalysis-eac4?tab=overview (accessed on 16 September 2021).
45. Rockel, B.; Will, A.; Hense, A. The regional climate model COSMO-CLM (CCLM). *Meteorol. Z.* **2008**, *17*, 347–348. https://doi.org/10.1127/0941-2948/2008/0309.
46. Doms, G.; Schättler, U. *A Description of the Nonhydrostatic Regional Model LM. Part I: Dynamics and Numerics*; Technical Report; Deutscher Wetterdienst: Offenbach, Germany, 2002.
47. Doms, G.; Foerstner, J.; Heise, E.; Herzog, H.J.; Mrionow, T.; Raschendorfer, D.; Reinhart, M.; Ritter, B.; Schrodin, R.; Schulz, J.P.; et al. *A Description of the Nonhydrostatic Regional COSMO Model. Part II: Physical Parameterization*; Technical Report; Deutscher Wetterdienst: Offenbach, Germany, 2011.
48. Baldauf, M.; Seifert, A.; Förstner, J.; Majewski, D.; Raschendorfer, M.; Reinhardt, T. Operational convective-scale numerical weather prediction with the COSMO model: Description and sensitivities. *Mon. Weather Rev.* **2011**, *139*, 3887–3905. https://doi.org/10.1175/MWR-D-10-05013.1.
49. Kinne, S. The MACv2 aerosol climatology. *Tellus B Chem. Phys. Meteorol.* **2019**, *71*, 1–21. https://doi.org/10.1080/16000889.2019.1623639.
50. Gelaro, R.; McCarty, W.; Suárez, M.J.; Todling, R.; Molod, A.; Takacs, L.; Randles, C.A.; Darmenov, A.; Bosilovich, M.G.; Reichle, R.; et al. The Modern-Era Retrospective Analysis for Research and Applications, Version 2 (MERRA-2). *J. Clim.* **2017**, *30*, 5419–5454. https://doi.org/https://doi.org/10.1175/JCLI-D-16-0758.1.
51. Kobayashi, S.; Ota, Y.; Harada, Y.; Ebita, A.; Moriya, M.; Onoda, H.; Onogi, K.; Kamahori, H.; Kobayashi, C.; Endo, H.; et al. The JRA-55 Reanalysis: General specifications and basic characteristics. *J. Meteor. Soc. Jpn.* **2015**, *93*, 5–48. https://doi.org/10.2151/jmsj.2015-001.
52. Harada, Y.; Kamahori, H.; Kobayashi, C.; Endo, H.; Kobayashi, S.; Ota, Y.; Onoda, H.; Onogi, K.; Miyaoka, K.; Takahashi, K. The JRA-55 Reanalysis: Representation of atmospheric circulation and climate variability. *J. Meteor. Soc. Jpn.* **2016**, *94*, 269–302. https://doi.org/10.2151/jmsj.2016-015.
53. Petrik, R.; Geyer, B.; Rockel, B. On the diurnal cycle and variability of winds in the lower planetary boundary layer: Evaluation of regional reanalyses and hindcasts. *Tellus A Dyn. Meteorol. Oceanogr.* **2021**, *73*, 1–28. https://doi.org/10.1080/16000870.2020.1804294.
54. Granier, C.; Darras, S.; van der Gon, J.D.; Doubalova, J.; Elguindi, N.; Galle, B.; Gauss, M.; Guevara, M.; Jalkanen, J.P.; Kuenen, J.; et al. *The Copernicus Atmosphere Monitoring Service Global and Regional Emissions*; Technical Report; Copernicus Atmosphere Monitoring Service (CAMS): Brussels, Belgium, 2019. https://doi.org/10.24380/d0bn-kx16.
55. Li, M.; Liu, H.; Geng, G.; Hong, C.; Liu, F.; Song, Y.; Tong, D.; Zheng, B.; Cui, H.; Man, H.; et al. Anthropogenic emission inventories in China: A review. *Natl. Sci. Rev.* **2017**, *4*, 834–866. https://doi.org/10.1093/nsr/nwx150.
56. Zheng, B.; Tong, D.; Li, M.; Liu, F.; Hong, C.; Geng, G.; Li, H.; Li, X.; Peng, L.; Qi, J.; et al. Trends in China's anthropogenic emissions since 2010 as the consequence of clean air actions. *Atmos. Chem. Phys.* **2018**, *18*, 14095–14111. https://doi.org/10.5194/acp-18-14095-2018.
57. Li, M.; Zhang, Q.; Streets, D.G.; He, K.B.; Cheng, Y.F.; Emmons, L.K.; Huo, H.; Kang, S.C.; Lu, Z.; Shao, M.; et al. Mapping Asian anthropogenic emissions of non-methane volatile organic compounds to multiple chemical mechanisms. *Atmos. Chem. Phys.* **2014**, *14*, 5617–5638. https://doi.org/10.5194/acp-14-5617-2014.
58. Li, M.; Zhang, Q.; Zheng, B.; Tong, D.; Lei, Y.; Liu, F.; Hong, C.; Kang, S.; Yan, L.; Zhang, Y.; et al. Persistent growth of anthropogenic non-methane volatile organic compound (NMVOC) emissions in China during 1990–2017: Drivers, speciation and ozone formation potential. *Atmos. Chem. Phys.* **2019**, *19*, 8897–8913. https://doi.org/10.5194/acp-19-8897-2019.
59. Liu, F.; Zhang, Q.; Tong, D.; Zheng, B.; Li, M.; Huo, H.; He, K.B. High-resolution inventory of technologies, activities, and emissions of coal-fired power plants in China from 1990 to 2010. *Atmos. Chem. Phys.* **2015**, *15*, 13299–13317. https://doi.org/10.5194/acp-15-13299-2015.
60. Tong, D.; Zhang, Q.; Liu, F.; Geng, G.; Zheng, Y.; Xue, T.; Hong, C.; Wu, R.; Qin, Y.; Zhao, H.; et al. Current Emissions and Future Mitigation Pathways of Coal-Fired Power Plants in China from 2010 to 2030. *Environ. Sci. Technol.* **2018**, *52*, 12905–12914. https://doi.org/10.1021/acs.est.8b02919.
61. Liu, J.; Tong, D.; Zheng, Y.; Cheng, J.; Qin, X.; Shi, Q.; Yan, L.; Lei, Y.; Zhang, Q. Carbon and air pollutant emissions from China's cement industry 1990–2015: Trends, evolution of technologies and drivers. *Atmos. Chem. Phys. Discuss.* **2020**, *2020*, 1–39. https://doi.org/10.5194/acp-2020-631.

62. Peng, L.; Zhang, Q.; Yao, Z.; Mauzerall, D.L.; Kang, S.; Du, Z.; Zheng, Y.; Xue, T.; He, K. Underreported coal in statistics: A survey-based solid fuel consumption and emission inventory for the rural residential sector in China. *Appl. Energy* **2019**, *235*, 1169–1182. https://doi.org/10.1016/j.apenergy.2018.11.043.
63. Crippa, M.; Solazzo, E.; Huang, G.; Guizzardi, D.; Koffi, E.; Muntean, M.; Schieberle, C.; Friedrich, R.; Janssens-Maenhout, G. High resolution temporal profiles in the Emissions Database for Global Atmospheric Research. *Sci. Data* **2020**, *7*, 1–17. https://doi.org/10.1038/s41597-020-0462-2.
64. Bieser, J.; Aulinger, A.; Matthias, V.; Quante, M.; Gon, H.A.D.V.D. Vertical emission profiles for Europe based on plume rise calculations. *Environ. Pollut.* **2011**, *159*, 2935–2946. https://doi.org/10.1016/j.envpol.2011.04.030.
65. Bieser, J.; Aulinger, A.; Matthias, V.; Quante, M.; Builtjes, P. SMOKE for Europe-adaptation, modification and evaluation of a comprehensive emission model for Europe. *Geosci. Model Dev.* **2011**, *4*, 47–68. https://doi.org/10.5194/gmd-4-47-2011.
66. Guenther, A.B.; Jiang, X.; Heald, C.L.; Sakulyanontvittaya, T.; Duhl, T.; Emmons, L.K.; Wang, X. The model of emissions of gases and aerosols from nature version 2.1 (MEGAN2.1): An extended and updated framework for modeling biogenic emissions. *Geosci. Model Dev.* **2012**, *5*, 1471–1492. https://doi.org/10.5194/gmd-5-1471-2012.
67. Guenther, A.; Jiang, X.; Shah, T.; Huang, L.; Kemball-Cook, S.; Yarwood, G. *Model of Emissions of Gases and Aerosol from Nature Version 3 (MEGAN3) for Estimating Biogenic Emissions*; Springer International Publishing: Berlin/Heidelberg, Germany, 2020; pp. 187–192.
68. MEGAN LAI. MEGAN, Leaf Area Index. 2021. Available online: https://bai.ess.uci.edu/megan/data-and-code/lai (accessed on 9 September 2021).
69. Baret, F.; Weiss, M.; Lacaze, R.; Camacho, F.; Makhmara, H.; Pacholcyzk, P.; Smets, B. GEOV1: LAI and FAPAR essential climate variables and FCOVER global time series capitalizing over existing products. Part1: Principles of development and production. *Remote Sens. Environ.* **2013**, *137*, 299–309. https://doi.org/10.1016/J.RSE.2012.12.027.
70. Jalkanen, J.P.; Brink, A.; Kalli, J.; Pettersson, H.; Kukkonen, J.; Stipa, T. A modelling system for the exhaust emissions of marine traffic and its application in the Baltic Sea area. *Atmos. Chem. Phys.* **2009**, *9*, 9209–9223. https://doi.org/10.5194/acp-9-9209-2009.
71. Jalkanen, J.P.; Johansson, L.; Kukkonen, J.; Brink, A.; Kalli, J.; Stipa, T. Extension of an assessment model of ship traffic exhaust emissions for particulate matter and carbon monoxide. *Atmos. Chem. Phys.* **2012**, *12*, 2641–2659. https://doi.org/10.5194/acp-12-2641-2012.
72. Johansson, L.; Jalkanen, J.; Kalli, J.; Kukkonen, J. The evolution of shipping emissions and the costs of regulation changes in the northern EU area. *Atmos. Chem. Phys.* **2013**, *13*, 11375–11389. https://doi.org/10.5194/acp-13-11375-2013.
73. Johansson, L.; Jalkanen, J.P.; Kukkonen, J. Global assessment of shipping emissions in 2015 on a high spatial and temporal resolution. *Atmos. Environ.* **2017**, *167*, 403–415. https://doi.org/10.1016/j.atmosenv.2017.08.042.
74. ECCAD. ECCAD-CAMS Global Emission Inventories. 2021. Available online: https://ads.atmosphere.copernicus.eu/cdsapp#!/dataset/cams-global-emission-inventories (accessed on 27 April 2022).
75. CIMAC. *Guide to Diesel Exhaust Emissions Control of NO_x, SO_x, Particulates, Smoke and CO_2*; Technical Report; The International Council on Combustion Engines (CIMAC): Frankfurt, Germany, 2008.
76. Zeretzke, M. Entwicklung Eines Modells zur Quantifizierung von Luftschadstoffen, die Durch Schiffsdieselmotoren auf See Emittiert Werden. Master's Thesis, Technische Universitat Hamburg-Harburg, Hamburg, Germany, 2013.
77. EMEP/EEA. *EMEP/EEA Air Pollutant Emission Inventory Guidebook 2019*; Technical Report; EMEP/EEA: Copenhagen, Denmark, 2019. https://doi.org/10.1017/CBO978 1107415324.004
78. Chen, D.; Wang, X.; Li, Y.; Lang, J.; Zhou, Y.; Guo, X.; Zhao, Y. High-spatiotemporal-resolution ship emission inventory of China based on AIS data in 2014. *Sci. Total Environ.* **2017**, *609*, 776–787. https://doi.org/10.1016/j.scitotenv.2017.07.051.
79. Fan, Q.; Zhang, Y.; Ma, W.; Ma, H.; Feng, J.; Yu, Q.; Yang, X.; Ng, S.K.; Fu, Q.; Chen, L. Spatial and Seasonal Dynamics of Ship Emissions over the Yangtze River Delta and East China Sea and Their Potential Environmental Influence. *Environ. Sci. Technol.* **2016**, *50*, 1322–1329. https://doi.org/10.1021/acs.est.5b03965.
80. Zhang, Y.; Fung, J.C.; Chan, J.W.; Lau, A.K. The significance of incorporating unidentified vessels into AIS-based ship emission inventory. *Atmos. Environ.* **2019**, *203*, 102–113. https://doi.org/10.1016/j.atmosenv.2018.12.055.
81. EEA. Air Quality e-Reporting (AQER). 2021. Available online: https://www.eea.europa.eu/data-and-maps/data/aqereporting-8 (accessed on 20 September 2021).
82. Yu, G.; Zhang, Y.; Yang, F.; He, B.; Zhang, C.; Zou, Z.; Yang, X.; Li, N.; Chen, J. Dynamic Ni/V Ratio in the Ship-Emitted Particles Driven by Multiphase Fuel Oil Regulations in Coastal China. *Environ. Sci. Technol.* **2021**, *55*, 15031–15039. https://doi.org/10.1021/acs.est.1c02612.
83. Shah, V.; Jacob, D.J.; Li, K.; Silvern, R.; Zhai, S.; Liu, M.; Lin, J.; Zhang, Q. Effect of changing NOx lifetime on the seasonality and long-term trends of satellite-observed tropospheric NO_2 columns over China. *Atmos. Chem. Phys.* **2020**, *20*, 1483–1495. https://doi.org/10.5194/acp-20-1483-2020.
84. Qi, Y.; Stern, N.; Wu, T.; Lu, J.; Green, F. China's post-coal growth. *Nat. Geosci.* **2016**, *9*, 564–566. https://doi.org/10.1038/ngeo2777.
85. Redl, C.; Hein, F.; Buck, M.; Graichen, D.P.; Jones, D. *The European Power Sector in 2020: Up-to-Date Analysis on the Electricity Transistion*; Technical Report; Agora Energiewende: Berlin, Germany, 2021.
86. IPCC. *Climate Change 1995*; Technical Report; IPCC: Geneva, Switzerland, 1995.
87. IPCC. *Climate Change, 2001*; Technical Report; IPCC: Geneva, Switzerland, 2001.

88. Li, K.; Jacob, D.J.; Liao, H.; Shen, L.; Zhang, Q.; Bates, K.H. Anthropogenic drivers of 2013–2017 trends in summer surface ozone in China. *Proc. Natl. Acad. Sci. USA* **2019**, *116*, 422–427. https://doi.org/10.1073/pnas.1812168116.
89. USEPA. *Integrated Science Assessment for Particulate Matter*; Technical Report; United States Environmental Protection Agency: Washington, DC, USA, 2009;
90. Baek, B.H.; Aneja, V.P.; Tong, Q. Chemical coupling between ammonia, acid gases, and fine particles. *Environ. Pollut.* **2004**, *129*, 89–98. https://doi.org/10.1016/j.envpol.2003.09.022.
91. Pathak, R.K.; Wu, W.S.; Wang, T. Summertime PM2.5 ionic species in four major cities of China: Nitrate formation in an ammonia-deficient atmosphere. *Atmos. Chem. Phys.* **2009**, *9*, 1711–1722. https://doi.org/10.5194/acp-9-1711-2009.
92. Seinfeld, J.H.; Pandis, S.N. *Atmospheric Chemistry and Physics: From Air Pollution to Climate Change*, 2nd ed.; Wiley: Hoboken, NJ, USA, 2006; p. 1232.
93. Chen, C.; Saikawa, E.; Comer, B.; Mao, X.; Rutherford, D. Ship Emission Impacts on Air Quality and Human Health in the Pearl River Delta (PRD) Region, China, in 2015, with Projections to 2030. *GeoHealth* **2019**, *3*, 284–306. https://doi.org/10.1029/2019GH000183.